# Quantifying the Importance of Selected Drought Indicators for the United States Drought Monitor

SONI YATHEENDRADAS,[a,c] DAVID M. MOCKO,[b,c] CHRISTA PETERS-LIDARD,[d] AND SUJAY KUMAR[b]

[a] *Earth System Science Interdisciplinary Center, University of Maryland, College Park, College Park, Maryland*
[b] *Science Applications International Corporation, Reston, Virginia*
[c] *Hydrological Sciences Laboratory, NASA Goddard Space Flight Center, Greenbelt, Maryland*
[d] *Sciences and Exploration Directorate, NASA Goddard Space Flight Center, Greenbelt, Maryland*

(Manuscript received 2 October 2022, in final form 28 March 2023, accepted 26 May 2023)

ABSTRACT: Using information theory, our study quantifies the importance of selected indicators for the U.S. Drought Monitor (USDM) maps. We use the technique of mutual information (MI) to measure the importance of any indicator to the USDM, and because MI is derived solely from the data, our findings are independent of any model structure (conceptual, physically based, or empirical). We also compare these MIs against the drought representation effectiveness ratings in the North America Drought Indices and Indicators Assessment (NADIIA) survey for Köppen climate zones. This reveals 1) agreement between some ratings and our MI values [high for example indicators like standardized precipitation evapotranspiration index (SPEI)]; 2) some divergences (e.g., soil moisture has high ratings but near-zero MIs for ESA Climate Change Initiative (CCI) soil moisture in the Western United States, indicating the need of another remotely sensed soil moisture source); and 3) new insights into the importance of variables such as snow water equivalent (SWE) that are not included in sources like NADIIA. Further analysis of the MI results yields findings related to 1) hydrological mechanisms (summertime SWE domination during individual drought events through snowmelt into the water-scarce soil); 2) hydroclimatic types (the top pair of inputs in the Western and non-Western regions are SPEIs and soil moistures, respectively); and 3) predictability (high for the California 2012–17 event, with longer-time scale indicators dominating). Finally, the high MIs between multiple indicators jointly and the USDM indicate potentially high drought forecasting accuracies achievable using only model-based inputs, and the potential for global drought monitoring using only remotely sensed inputs, especially for locations having insufficient in situ observations.

SIGNIFICANCE STATEMENT: Drought maps from the U.S. Drought Monitor and the Objective Short- and Long-Term Drought Indicator Blends and Blend Equivalents are integrated information sources of the different types of drought. Multiple indicators go into creation of these maps, yet it is usually not clear to both public and private stakeholders like local agencies and insurance companies about the importance of any indicator in any region and season to the drought maps. Our study provides such objective information to enable understanding the mechanism and type of drought occurring at a location, season, and possibly event of interest, as well as to potentially aid in better drought monitoring and forecasting using smaller custom sets of indicators.

KEYWORDS: Drought; Entropy; Hydrology; Statistical techniques; Decision support; Other artificial intelligence/machine learning

## 1. Introduction

Drought happens on a variety of time scales and is of multiple types that can be either physical in nature (meteorological, agricultural, hydrological, and ecological) or socioeconomic. Over the continental United States, the U.S. Drought Monitor (USDM) is widely recognized as the definitive current monitoring source providing combined information on the onset, severity, extent, and recovery for multiple types of drought. Separated information on short- and long-term droughts is provided by the Objective Drought Indicator Blends and Blend Equivalents from the Climate Prediction Center and from the National Drought Mitigation Center. For its representation of short- and long-term droughts, the NOAA (2023) survey has consistently rated USDM as effective or very effective (a 4–5 rating out of a maximum of 5) in all Köppen climate zones (Critchfield 1974; WMO and GWP 2016; Beck et al. 2018). The USDM is constructed using a combination of expertise, experience and indicators-based objective information by a centralized group of USDM authors (Svoboda et al. 2002).

Improved drought communications and decision-making for stakeholders, end-users, and the general public will be facilitated by the knowledge of the magnitude by which different physical mechanisms affect the determination of drought. One way to know this is by determining the drought representativeness of individual or set of indicators reflecting such mechanisms for any location and season (Heim 2002; Zargar et al. 2011). Toward this

Supplemental information related to this paper is available at the Journals Online website: https://doi.org/10.1175/JHM-D-22-0180.s1.

*Corresponding author*: Soni Yatheendradas, soni.yatheendradas@nasa.gov

DOI: 10.1175/JHM-D-22-0180.1

© 2023 American Meteorological Society. This published article is licensed under the terms of the default AMS reuse license. For information regarding reuse of this content and general copyright information, consult the AMS Copyright Policy (www.ametsoc.org/PUBSReuseLicenses).

Brought to you by NOAA Central Library | Unauthenticated | Downloaded 08/13/24 07:18 PM UTC

goal, recent tools like the Drought Risk Atlas (Svoboda et al. 2015) provide plots of the USDM alongside conventional indicators such as the standardized precipitation index (SPI) and the Palmer drought severity index (PDSI) at any location of interest. While this atlas is useful in a qualitative sense, we seek traceability of common information between specific indicators and the USDM. Quantitative knowledge is also critical for the development of optimized custom objective blends for more accurate drought early warning systems.

A fundamental approach to determine the relative importance of an indicator variable for a target variable (here, the USDM) is to start with the informatic theoretic concept of entropy, which is the information content or uncertainty in that variable (Shannon 1948a,b; also, see the appendix for some explanation of information theory metrics). The earliest entropy application in physical and Earth sciences was by Leopold and Langbein (1962), who found the most probable description of a longitudinal river profile. Since then, there have been many applications of entropy in hydrology, hydrometeorology, and hydroclimatology, some of which are Sonuga (1972) in hydrologic frequency analysis; Dalezios and Tyraskis (1989), Maruyama and Kawachi (1998), and Maruyama et al. (2005) in precipitation analysis and distributions; Krasovskaia (1995, 1997) in typology of river runoff regimes; Cheng et al. (2004) and Fleming (2007) in air quality analysis; and Wrzesinski (2016) in river runoff. The common entropic information between two variables is called mutual information (MI; Shannon 1948a,b; Kreer 1957; also, see the appendix). Mutual information has similarly been used in multiple applications, for example, modeled versus observed streamflows by Amorocho and Espildora (1973), observed streamflows within a watershed by Caselton and Husain (1980) and Yang and Burn (1994), air quality by Jain and Sharma (2003), and assimilation of satellite remotely sensed soil moisture into a land surface model by Nearing et al. (2018). Relevant to our study, MI is the amount of information obtained about the USDM by observing the other indicator. Another information theoretic metric complementary to mutual information is conditional entropy—that is, the residual information of one variable given the knowledge of another variable (see the appendix). Example studies of this include Sonuga (1976) on the rainfall–runoff process, Krasovskaia (1997) on river runoff regimes, and Majda and Gershgorin (2010) on climate change modeling.

In the literature mentioned above, MI is calculated between continuous or real-valued variables. However, our study differs in that the MI is calculated between *a discrete variable like the USDM* (five categories, from abnormally dry to exceptional drought) *and a continuous variable* (our study's indicators that reflect the inputs contributing to the USDM), for which we use the Ross (2014) nearest neighbor distance-based technique of robust and accurate MI calculation. Ross (2014) designated MI to be a perfect statistic for measuring the amount of relatedness between variables due to its comprehensiveness, interpretability, and insensitivity to data sample size. Comprehensiveness denotes the ability of MI to capture all the moments of the relationship instead of only selected lower moments like mean and/or variance captured by most statistical measures. The interpretability reflects the established foundation of theoretical tools on which information entropy is based. Finally, the insensitivity to sample size refers to convergence with tight error bounds, unlike other statistical techniques where an independence between even slightly related variables is determined by a significance test wherein the $p$ values can be made arbitrarily low by considering a large sample size. Our study uses MI because it is *derived solely from the data and is thus independent of any model structure* (conceptual, physically based, or empirical). The main disadvantage faced by MI and other information theory metrics is that the computational costs can be high.

During the MI calculation, we use percentiles for each indicator instead of their values, to conform to the typical use of percentiles in drought monitoring and prediction. Since the USDM drought entropies and consequently the MI values can vary spatially, we divide the MI value by the USDM entropy to obtain the fractional information (FI) values that enable comparison across spatial domains (see appendix).

The calculated FIs enable investigating our first two study questions:

1) How do these FIs compare against the community consensus ratings of the drought indicators?
2) Do they provide any process insights?

Our *continuous variable* can be either a *single indicator* or a *set* of indicators that jointly form a multivariate or *multidimensional* indicator.

For such a multidimensional indicator, the percentile calculation on each of its individual indicators fortuitously scales that indicator's values into the same range as of the other indicators. This same range avoids imparting preferential biases during the nearest neighbor distance-based MI calculation in multidimensional space due to different orders of magnitude of the values among the indicators.

The *FI calculation* between any *multidimensional indicator* and the USDM provides an "*upper bound*" on the possible *accuracy* obtainable with that set of indicator inputs in reproducing the USDM maps using any *model-based prediction* techniques (e.g., machine learning using convolutional neural networks or random forests). This makes the knowledge gained from this FI analysis *relevant to both monitoring and prediction efforts of drought* as captured by USDM. Thus, there are two remaining questions explored in our study:

3) Can indicators obtained from a model run in turn potentially provide accurate drought forecasts?
4) Can a drought monitor constructed using only remotely sensed inputs effectively function even within in situ data-scarce locations?

## 2. Materials and methods

The following subsections illustrate the different aspects of the overall data flow and experimental design of this study illustrated in Fig. 1. Steps include first spatially interpolating or aggregating all the data to the resolution of Climate Divisions, then temporally interpolating or aggregating the indicators to the weekly resolution of the USDM maps, and finally calculating the

Brought to you by NOAA Central Library | Unauthenticated | Downloaded 08/13/24 07:18 PM UTC

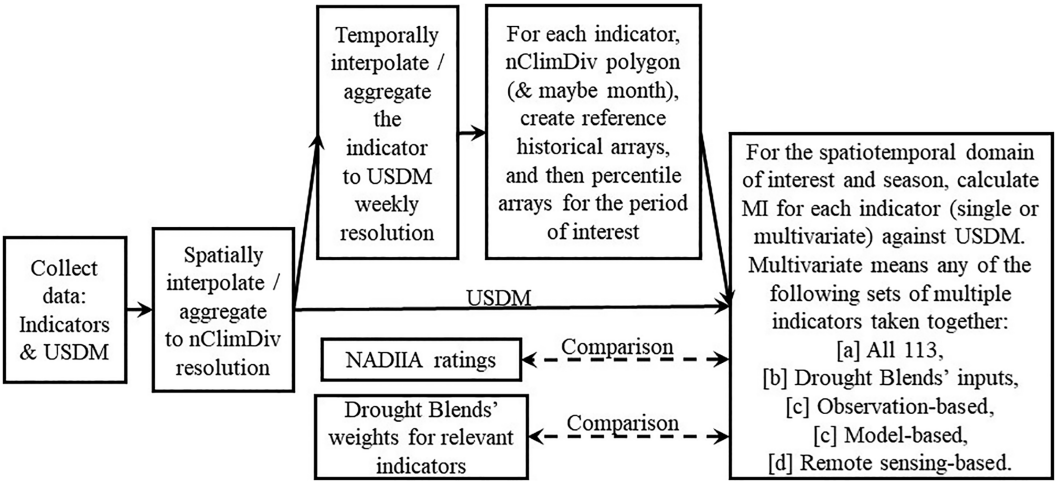



FIG. 1. The overall data flow and experimental design of this study.

indicator percentiles to calculate their MI values and maybe compare against existing weights or ratings.

### a. *Spatial analytic regions*

Spatial domains analyzed in this study include the entire CONUS (contiguous United States) spanned by the Objective Short-Term Drought Indicator Blend from the Climate Prediction Center (CPC) (NOAA/CPC 2021). The two CPC Objective Long-Term Drought Indicator Blends span the Western and the non-Western United States, respectively (Fig. 2a), that together form the CONUS domain. Hereafter we refer to the CPC Objective Short- and Long-Term Drought Indicator Blends as simply the CPC Short- and Long-Term Blends, respectively. The entire CONUS (for Short-Term) and the Western and non-Western U.S. domains (for Long-Term) were also used for the initial version of the Short- and Long-Term Objective Drought Indicator Blend Equivalents from the National Drought Mitigation Center (NDMC; UNL 2021b). Similar to the CPC Blends, we hereafter refer to these latter Blend Equivalents as the NDMC Short- and Long-Term Blends. Note that we refer to the "non-Western" U.S. domain that way and not "Eastern" because it contains some westernmost portion of Washington State and Oregon.

Our study also analyzes six USDM regions that also together form the CONUS domain. UNL (2021a) provides the weekly USDM drought summary for these regions, where the states of Wyoming and Colorado are included in both the West and the High Plains regions (Fig. 2b). Note that the USDM High Plains region is split between the CPC Western and non-Western regions. Each USDM region spans multiple states, and each state spans multiple Climate Division polygons (nClimDiv: NOAA/NCDC 2021; Vose et al. 2014a,b; see Fig. 2c). The CPC Blends are available at this nClimDiv resolution (abbreviated nCD in the figures), and our study also prepares the indicators at the same resolution; however, we use these nClimDiv resolution values to calculate the MI values at the coarser CPC and USDM regional domain resolutions for the 2006–19 period.

### b. *Selected indicators and the USDM*

Table 1 lists the spatiotemporal properties, time durations, and time scales considered for our study's large set of indicators. The set of indicators used was subjectively developed based on 1) our difficulty in obtaining the most up-to-date list of indicators going into the USDM creation process at the time that we started our study, 2) our available computation and time resources in processing all the data, and 3) our attempt to have a list of indicators that is as representative as possible of the current landscape of indicators. Some popular datasets were not included, for example, SMAP soil moisture because its short duration was not enough to satisfactorily capture climatological behavior and calculate percentiles. The Short- and Long-Term Blends from the CPC and the NDMC each are created from their respective sets of 5–6 indicator inputs (shown later in Table 2). Our study initially shows some results for these sets of Blends' inputs before showing results from our full nonexhaustive set of 113 indicators and its other subsets. For precipitation in this initial part, we accordingly use the nClimDiv resolution precipitation (row 4 in Table 1) from the subsets of indicators forming the CPC Blends' inputs, but the approximately 5-km latitude/longitude nClimGrid resolution precipitation otherwise (NOAA/NCEI 2021a; it is still converted to our study's nClimDiv resolution).

Among the mainly observation-based indicators used in our study, NOAA/NCEI (2021a) provide datasets of precipitation, air temperatures, SPI, and SPEI (standardized precipitation evapotranspiration index) (rows 1–3 of Table 1) at the nClimGrid resolution (abbreviated nCG in the figures). The quality control and spatial interpolation methodology during their creation is the same as that typically followed for the nClimDiv resolution (Vose et al. 2014a). The SPEI differs from SPI in replacing the precipitation with the difference between precipitation and potential evapotranspiration as a representation of a simple climatic water balance. Note that while the nClimGrid SPI and SPEI each are available at both the Pearson and gamma distributions, our figures show the

Brought to you by NOAA Central Library | Unauthenticated | Downloaded 08/13/24 07:18 PM UTC

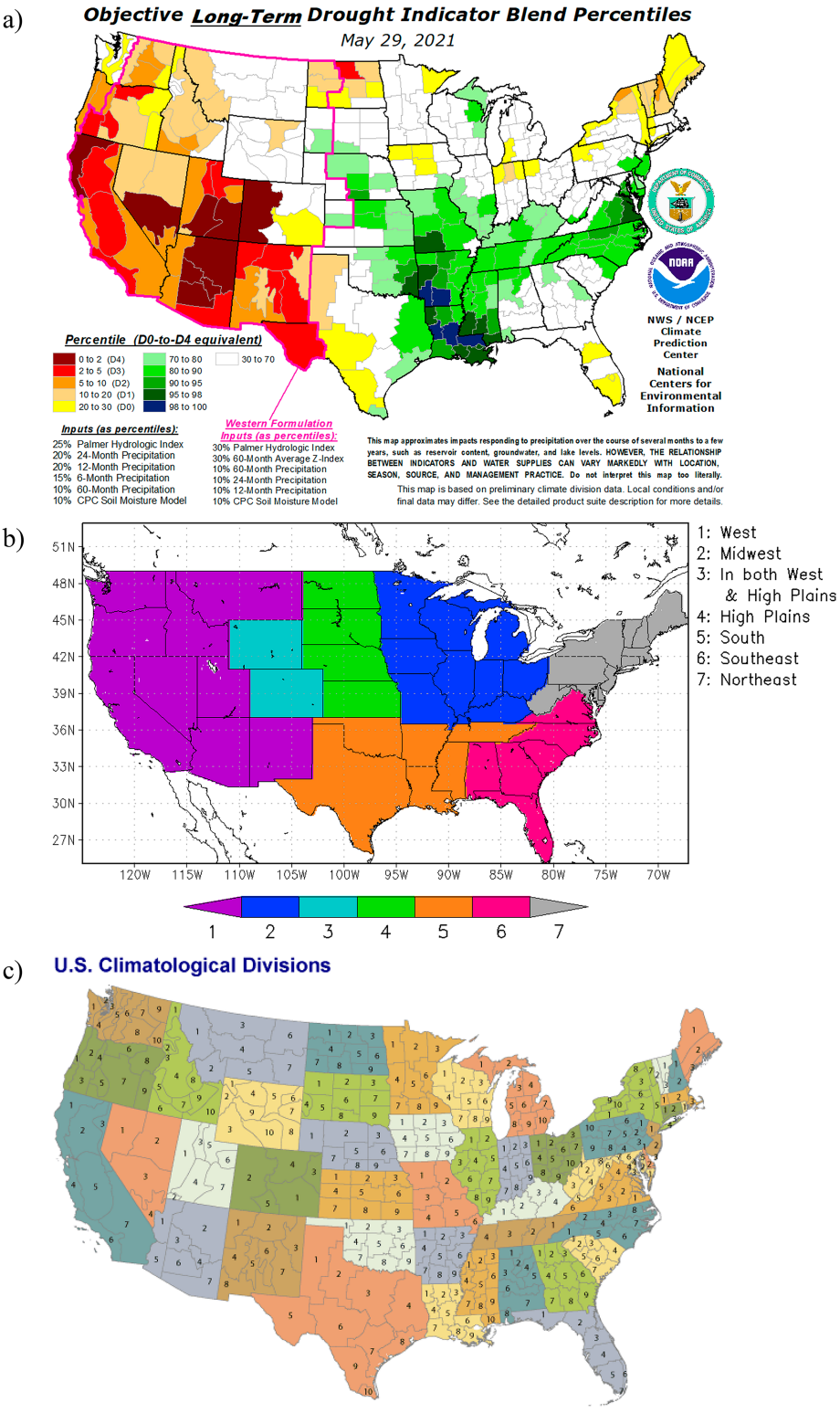



FIG. 2. (a) Spatial domains occupied by the CPC Long-Term Blends as well as the NDMC Long-Term Blends over CONUS. Note that the non-Western U.S. region (see the Western region delineated by bright pink boundary) also includes portions of coastal Washington and Oregon. (b) The spatial domains of the USDM regions. (c) The U.S. Climate Divisions. Panels reproduced from NOAA/NCDC (2021), NASA/GSFC (2021), and Drought.gov (2021), respectively.

Brought to you by NOAA Central Library | Unauthenticated | Downloaded 08/13/24 07:18 PM UTC

TABLE 1. Drought indicators considered in this study. Subsets in the table are based on considering each drought indicator to be mainly observation, model, or remotely sensed based. Model based refers to conceptual or physically based models and not statistical models. This study uses the CPC nClimDiv-resolution precipitation drought indicator (row 4) in only the subsets forming Blends' inputs, otherwise it uses the NCEI precipitation (row 1) for the complete set of drought indicators or its other subsets.

| No. | Drought indicators | Spatial resolution | Time resolution | Data period | No. of inputs (averaging periods) |
|---|---|---|---|---|---|
| | Mainly observation based (total of 39, excluding the CPC Blends' precipitations) | | | | |
| 1 | Precipitation (NCEI) | nClimGrid | Monthly | 1895–2020 | 11 (1, 2, 3, 6, 9, 12, 24, 36, 48, 60, and 72 months) |
| 2 | SPI and SPEI (NCEI) | nClimGrid | Monthly | 1895–2020 | 22 (1, 2, 3, 6, 9, 12, 24, 36, 48, 60, and 72 months) |
| 3 | Mean and maximum air temperature (NCEI) | nClimGrid | Monthly | 1895–2020 | 2 |
| 4 | Precipitation (CPC Blends) | nClimDiv | Monthly | 1932–2019 | 6 (1, 3, 6, 12, 24, and 60 months) |
| 5 | *Z* indices (Palmer) | nClimDiv | Monthly | 1932–2019 | 2 (1 and 60 months) |
| 6 | PMDI (Palmer modified drought index) | nClimDiv | Weekly | 2005–19 | 1 |
| 7 | PHDI (Palmer hydrologic drought index) | nClimDiv | Weekly | 2005–19 | 1 |
| | Mainly model based (total of 53) | | | | |
| 8 | NLDAS-2 percentiles:<br>• Top 1-m soil moisture<br>• Total column soil moisture<br>• Evapotranspiration<br>• SWE (snow water equivalent)<br>• Total runoff<br>• Streamflow<br>For each of the four LSMs (Mosaic, Noah, SAC, VIC) | 0.125° | Daily | 1980–2020 | 24 |
| 9 | GRACE DA percentiles:<br>• Top 1-m soil moisture<br>• Total column soil moisture<br>• Groundwater | 0.125° | Weekly | 2002–19 | 3 |
| 10 | EDDI (evaporative demand drought index) | 0.125° | Daily | 1980–2020 | 24 (1–12 weeks and 1–12 months) |
| 11 | CPC soil moisture | 1.0° | Daily | 2008–19 | 1 |
| 12 | SNODAS (SWE) | 0.0083° (1 km) | Daily | 2003–20 | 1 |
| | Mainly remote sensing based (total of 18) | | | | |
| 13 | IMERG precipitation | 0.1° | Daily | 2000–20 | 11 (1, 2, 3, 6, 9, 12, 24, 36, 48, 60, and 72 months) |
| 14 | ESA CCI soil moisture | 0.25° | Daily | 1979–2020 | 1 |
| 15 | GlobSnow3 (SWE) | 0.25° | Daily | 1979–2018 | 1 |
| 16 | ESI (evaporative stress index) | 0.04° | Daily | 2000–19 | 2 (4 and 12 weeks) |
| 17 | Blended-VHP (NDVI, TCI, VCI, and VHI) | 0.036° (4 km) | Weekly | 1981–2020 | 1 |
| 18 | VegDRI | 0.01° (1 km) | Weekly | 2000–20 | 4 |
| 19 | QuickDRI | 0.01° (1 km) | Weekly | 2009–20 | 1 |

results using the SPI with gamma distribution and the SPEI with Pearson distribution. However, we briefly report in the results in section 3e about the almost negligible sensitivity to the statistical distribution used.

NOAA/NCEI (2021b) produces monthly nClimDiv resolution precipitation and Palmer *Z* index (rows 4–5 of Table 1) that are used in the CPC Blends' creation process. This Palmer *Z* index is a byproduct during the production of the PDSI that aims to characterize the duration and intensity of the long-term drought-causing circulation patterns (Palmer 1965). The first of our two weekly nClimDiv resolution indicators (rows 6–7 of Table 1) is the Palmer modified drought index (PMDI; Heddinghaus and Sabol 1991), which is an operational version of PDSI. The other one is the Palmer hydrological drought index (PHDI; Heim 2005) that additionally incorporates into PDSI the attenuating effects of hydrological stores toward responding slower to changing conditions than PDSI.

Next are mainly model-based indicators on rows 8–12 of Table 1, starting with the NLDAS-2 variables of land surface models' states and outputs that were also used in the drought blend study by Xia et al. (2014). The Gravity Recovery and Climate Experiment (GRACE) data assimilation (DA) data (Houborg et al. 2012; Zaitchik et al. 2008) are obtained from

Brought to you by NOAA Central Library | Unauthenticated | Downloaded 08/13/24 07:18 PM UTC

TABLE 2. Drought indicators used in the CPC and NDMC Short- and Long-Term Blends (both Western and non-Western formulations). Note that five drought indicators are used for the Short-Term Blends while six drought indicators are used for the Long-Term Blends. Values in parentheses represent the percentage weight of that indicator used in each Blend.

| CPC Short-Term | NDMC Short-Term | CPC Long-Term Western | NDMC Long-Term Western | CPC Long-Term non-Western | NDMC Long-Term non-Western |
|---|---|---|---|---|---|
| Palmer Z index (35%) | 1-month SPEI (35%) | PHDI (30%) | 9-month SPEI (30%) | PHDI (25%) | 9-month SPEI (25%) |
| 3-month nClimDiv precipitation (25%) | 3-month SPI (25%) | 60-month *Z* index (30%) | 60-month SPEI (30%) | 24-month nClimDiv precipitation (20%) | 24-month SPI (20%) |
| 1-month nClimDiv precipitation (20%) | 1-month SPI (20%) | 60-month nClimDiv precipitation (10%) | 60-month SPI (10%) | 12-month nClimDiv precipitation (20%) | 12-month SPI (20%) |
| CPC soil moisture (13%) | Noah 0–100-cm soil moisture (13%) | 24-month nClimDiv precipitation (10%) | 24-month SPI (10%) | 6-month nClimDiv precipitation (15%) | 6-month SPI (15%) |
| PMDI (7%) | 9-month SPI (7%) | 12-month nClimDiv precipitation (10%) | 12-month SPI (10%) | 60-month nClimDiv precipitation (10%) | 60-month SPI (10%) |
| | | CPC soil moisture (10%) | Noah 0–200-cm soil moisture (10%) | CPC soil moisture (10%) | Noah 0–200-cm soil moisture (10%) |

assimilations of the terrestrial water storage observations from the GRACE sensor into the Catchment land surface model (CLSM). The EDDI data (evaporative demand drought index; Hobbins et al. 2016; McEvoy et al. 2016) capture atmospheric evaporative demand. We use the daily, 1° CPC soil moisture that is one input to the CPC Blends (van den Dool et al. 2003). The Snow Data Assimilation System (SNODAS; NOHRSC 2004) provides snow water equivalent (SWE) estimates.

Last, our study also includes remote sensing–based indicators (rows 13–19 of Table 1), starting with precipitation from IMERG (Integrated Multi-satellitE Retrievals for GPM; Huffman et al. 2014), where GPM denotes the Global Precipitation Measurement satellite constellation. The ESA Climate Change Initiative (CCI) soil moisture product version v06.1 (Dorigo et al. 2017; Gruber et al. 2019; Preimesberger et al. 2021) combines information from active scatterometer and passive radiometer sensors. GlobSnow3 (Luojus et al. 2020; Pulliainen et al. 2020) is version 3.0 of the SWE data produced by a combination of satellite-based passive microwave radiometer data (*Nimbus-7* SMMR, DMSP 5D2 SSM/I, and DMSP 5D3 SSMIS) with ground based synoptic snow depth observations using Bayesian data assimilation into a snow emission model.

Among vegetation-related indicators, the ESI (evaporative stress index; Anderson et al. 2007) combines atmospheric evaporative demand with vegetation to capture vegetative stress and is basically evapotranspiration (ET) normalized by a reference or potential ET. The blended-VHP (blended vegetation health product: NOAA/NESDIS 2021) is a reprocessed dataset from VIIRS (2013–present) and AVHRR (1981–2012) data and contains multiple variables of which our study uses NDVI (normalized difference vegetation index), TCI (temperature condition index), VCI (vegetation condition index), and VHI (vegetation health index). Note that this product having "blended" in its name is unrelated to the Short- and Long-Term Objective "Blends." The VegDRI product (vegetation drought response index; Brown et al. 2008) depicts vegetation stress response over a seasonal 6–9-month period to solar energy, soil moisture, and other limiting factors by integrating satellite-based observations of vegetation conditions, climate data, and other biophysical information such as land cover/land use type, soil characteristics, and ecological setting. In contrast to the VegDRI, the QuickDRI (quick drought response index; Wardlow et al. 2017) is a shorter-term indicator (~1 month) of dryness and environmental stress to detect rapid-onset "flash drought" events having devastating economic impacts on specifically the agricultural sector, and is an analysis of satellite- and model-based observations.

Table 2 lists the drought indicators used as inputs for creating the CPC and NDMC Blends. The inputs in the initial version of these NDMC Blends seem to have followed a systematic rule-of-thumb so that there is an almost one-to-one equivalence with the CPC Blends' inputs: the *Z* indices (1 and 60 months) with the corresponding time scale nClimGrid resolution SPEIs, the CPC precipitation (1, 3, 6, 12, 24, and 60 months) with the corresponding time scale nClimGrid SPIs, the PMDI with the 9-month nClimGrid SPI, the PHDI with the 9-month nClimGrid SPEI, and the CPC soil moisture with either the Noah 0–100-cm (root zone) moisture in the NDMC Short-Term Blend or the Noah total column (0–200 cm) soil moisture in the NDMC Long-Term Blend. Note that the SPEIs in the NDMC Blends have a three-parameter log-logistic distribution (Vicente-Serrano et al. 2010; Beguería et al. 2014), in contrast with the NCEI nClimGrid SPEIs available at Pearson and gamma distributions.

The weekly USDM maps from UNL (2021a) are polygon shapefiles. For obtaining drought category values at the nClimDiv resolution (see section 2a), we areally intersected the USDM and nClimDiv shapefiles to obtain the areas occupied by the drought categories in each Climate Division and then assigned the maximum-area category to that Climate Division. Most indicators were not available at the nClimDiv resolution and so were first converted to the GeoTiff format. Next, for indicators with native resolution coarser than 4 km, we converted the GeoTiff rasters to grid polygons, spatially intersected them with nClimDiv polygons and then performed area-weighting to obtain the nClimDiv resolution values. For indicators finer

Brought to you by NOAA Central Library | Unauthenticated | Downloaded 08/13/24 07:18 PM UTC

than 4-km resolution, we simply averaged the GeoTiff pixel values situated in each nClimDiv polygon. Next, we processed the indicators to the same time resolution and week definition as the USDM maps by interpolating when the native resolution is weekly (for week ending-day definitions different from that of a USDM week) or coarser, else accumulating/averaging when it is finer.

We then map these converted indicator values to percentiles, for which the reference arrays of each indicator were taken to be either a single overall array for all months together, or separate monthly arrays. For indicators having values at multiple time scales, namely, precipitation, SPIs, SPEIs, and EDDIs, we used monthly reference arrays for time scales of less than 12 months, otherwise we used overall arrays. We took overall reference arrays for the Palmer indices (PMDI, PHDI, and *Z* indices), snow, runoff, streamflow, and GRACE DA groundwater indicators, and monthly arrays for the ESI, blended-VHP, and NLDAS-2 evapotranspiration indicators. The soil moistures (CPC, 1-m or root zone, and total column) were subject to monthly reference arrays, except for the ESA CCI product for which we used the overall array since it had lot of data gaps. Note that this reference array treatment of monthly versus all months together differs from the reporting of results in our study for the 3-month seasons of winter (December–February), spring (March–May), and so on, besides reporting for all seasons taken together.

Some indicators in Table 1 had additional preprocessing before the percentile calculation. The NLDAS-2 streamflows had noticeable nonzero values only along pixels of the river network that was constructed using a DEM to determine the flow direction for each 0.125° NLDAS pixel (Lohmann et al. 2004). Because of the conceptual understanding that the streamflow value at any point is an integrated value coming from a group of contiguous upstream pixels, we assigned the daily mean of the streamflow pixel values in each HUC04-level (Hydrologic Unit Code) discretization of watersheds to those streamflow pixels. The GlobSnow3 input had gaps every year from approximately the beginning of May to the end of October, during which we simply assumed zero values everywhere. The CPC soil moisture presented the most challenges, with the data timeline revealing multiple data gaps and variations in the formats and data grid specifications for both the daily and monthly data (see Fig. S1 in the online supplemental material). We wrote a data reader in the Python language to handle these challenges.

Even though the available data record of PMDI, PHDI, and CPC soil moisture might not be sufficiently long climatologically, our study assumes that their shorter periods overlapping with the USDM maps suffice to calculate the input percentiles. The time period of concurrent availability (with possible gaps) of the indicators and the USDM required for our information theoretical analysis then starts only from February 2008 onward due to the CPC soil moisture data available only thereafter. Additionally, in the absence of data availability at weekly or finer time scales of the Palmer *Z* indices, CPC Blends' precipitation, and the NCEI indicators, we assume that instead our interpolation of their monthly values to weekly will suffice. Note that the monthly Palmer values can sometimes paint contrasting drought pictures against weekly (Heim 2005) because monthly values might not capture some interweekly patterns of interest.

### c. *Code for calculating mutual information*

The available supplemental material codes with the Ross (2014) article provide a MATLAB language code implementation of MI calculation between any continuous variable and discrete variable, where each input can be either univariate or multivariate/multidimensional. To avoid MATLAB licensing issues for distributed MI runs on multiple processors, we used the available "mutual_info_classif" function in the Python language-based scikit-learn machine learning module for the univariate case. For the multivariate indicator case, we recoded the MATLAB code into Python to create a custom multivariate continuous-variable adaptation of this mutual_info_classif function with the same code structure and calling interface. Both the mutual_info_classif function and its multivariate continuous-variable adaptation have a random seed as an input argument or parameter that provide a small uncertainty to the MI. Each reported MI in our results is the median value from among 101 MI calculations corresponding to as many random seeds.

### d. *Comparison of FI values against the NADIIA survey*

To compare our FI values against some broad scientific or community consensus, we consider the NOAA (2023) results from the North America Drought Indices and Indicators Assessment (NADIIA) survey of drought users and stakeholders about the effectiveness of indicators usually considered in drought monitoring and forecasting. This effectiveness is spatially characterized over Köppen climate zones in the form of distributions of subjective ratings from 1 to 5 (i.e., less to very effective). The Köppen climate classification system is one of the oldest and most widely used (Critchfield 1974; WMO and GWP 2016; Beck et al 2018; NOAA 2023). Among the unique climate zones over CONUS, those starting with the letter A are tropical, B are dry, C are temperate, and D are continental, where mountainous snow and ephemeral ponds are supplied by groundwater or permafrost. We now look at the presence of Köppen zones within the USDM regions to enable connecting our MI calculations at the USDM regional scale with the NADIIA ratings for Köppen zones.

The A zones occupy very tiny areas and are in the USDM Southwest region. The B zones exist in the South and West regions, with specifically the BSk zone (cold semiarid climate) also existing in the High Plains. The temperate Mediterranean Cs zones are summer Mediterranean climates and occur in the West, while the Cfa is a humid subtropical climate that occurs in all regions and covers most of the South and almost all of Southeast but is a very tiny area in the West. Also, the Cfb temperate oceanic climate occupies only a little area in all regions except the High Plains and Midwest where it does not exist. The Ds dry summer–based humid continental climate zones (Dsa and Dsb) are situated in the West with Dsa (humid continental climate—dry warm summer) spanning only a little area. The Dwa zone (humid continental hot summers with dry

Brought to you by NOAA Central Library | Unauthenticated | Downloaded 08/13/24 07:18 PM UTC

TABLE 3. Spatiotemporal domain of individual drought events considered in this study.

| No. | Event | Time period considered | Spatial domain considered |
|---|---|---|---|
| 1 | Northern Plains 2017 | 25 Apr 2017–10 Apr 2018 | Montana and both Dakotas |
| 2 | California 2012–17 | 3 Jan 2012–7 Feb 2017 | California |
| 3 | Midwest/Central U.S. 2012 | 19 Jun 2012–28 May 2013 | USDM regions of High Plains, Midwest, South |
| 4 | Texas 2011 | 7 Dec 2010–15 May 2012 | Texas, Oklahoma, New Mexico |
| 5 | Southeast 2006–08 | 24 Apr 2007–1 Apr 2008 | Mississippi + USDM Southeast region |

winters) exists only in the High Plains region. Most of the Northeast region is occupied by the Dfb zone (humid continental mild summer, wet all year). Summarizing all this information to find the zones that occupy most or all of any USDM region, the only zones for which we can conclude about the indicator importances based on the results of the USDM regions are Cfa (corresponding to the USDM South and Southeast regions) and Dfb (the USDM Northeast region).

As shown later in this study, our obtained FI values are less than 40% except for a few "outliers" falling in the 40%–50% range. A fairer and objective comparison between the FIs and the NADIIA ratings would have split the FI range of 0%–100% into five consecutive ranges (say, 0%–20%, 20%–40%, and so on that would have assigned the outlier values into the middle 40%–60% range and the rest into lower ranges). This would likely almost always provide a big contrast between the FI ranges and the NADIIA ratings. However, we assume that a practically more useful comparison is when the FI values are considered in a relative fashion to each other and assigned to ranges so that all ranges have values present like the NADIIA ratings have. Hence, we subjectively consider consecutive intervals of 8% and starting at 0% for assigning the ranges, with values above 40% also assigned to the uppermost range of 32%–40%. A low FI value of around less than 16% then puts it in the bottom two-fifths range of FI values and will contrast with a NADIIA rating of 4–5. Similarly, an FI of greater than around 24% puts it in the top two-fifths range of FI values and will contrast with a NADIIA rating of 1–2.

### e. *Specific drought events considered*

This subsection describes more limited spatiotemporal domains of interest considered in this study other than the ones mentioned in section 2a. Droughts are often perceived as slow-moving natural hazards, so the phenomenon of flash droughts in the last couple of decades has attracted increasing attention. These flash droughts rapidly develop or intensify within a short period from 5 days to 8 weeks, yet there is no consensus on their exact definition (NOAA/NIDIS 2021). However, in addition to below-normal precipitation that usually causes regular drought, flash droughts are additionally characterized by the important requirement of high evaporative demand (Otkin et al. 2018).

Existing products for monitoring and forecasting of flash drought are typically inadequate. For example, during such droughts, the USDM apparently did not adequately monitor local conditions existing on the ground, or lagged local conditions (Woloszyn et al. 2021). Further, CPC's monthly drought outlook product failed to forecast the 2017 flash drought over the Northern Great Plains, for which Hoell and Wang (2021) mentioned changes in ET as an important indicator variable to consider for early warning. Woloszyn et al. (2021) has explicitly pointed out the importance of studying the changes in flash drought indicator values such as precipitation, evaporative demand, soil moisture, evapotranspiration, and vegetation health for successfully monitoring flash drought, in addition to studying these values themselves. Note that our study looks only at the values and not their temporal changes as separate indicators. For the latter, past studies have used evaporation/ET, soil moisture, precipitation, temperature, USDM, and NDVI in decreasing order of frequency to define flash drought (NOAA/NIDIS 2021). Table 3 lists the considered spatiotemporal domains for the following five specific well-known drought events considered in this study, most of which had at least a significant flash drought component.

The first event is the 2017 Northern Plains flash drought that was associated with fires that burned 4.8 million acres (NOAA/NIDIS 2019a,b). The causes of this event in the spring and summer of 2017 were very high temperatures and record low precipitation resulting in the near-record rapidity of the soil moisture decline after high amounts of SWE in fall 2016 (Hoell et al. 2019; Downey 2020). However, the USDM maps for this event indicate that drought started only at the end of spring (late May) 2017. Next is the 2011–17 California drought that was the driest period in California's recorded history and was caused by a ridge of high pressure in the Pacific Sea called the "ridiculously resilient ridge" (Swain et al. 2014; Bond et al. 2015).

The third drought event considered is in 2012 in the Midwest/Central United States and is actually a part of the 2012/13 North American drought that in turn is an expansion of the 2010–13 southern United States drought (Freedman 2012a,b). This drought was initiated due to the conditions from the Arctic and North Atlantic oscillations during the winter of 2011/12 (Lindsey 2011). The drought over the Midwest was mostly over by 26 March 2013, but persisted in the central United States until late May 2013. Per Woloszyn et al. (2021), the Central U.S. portion of this flash drought "affected approximately 80% of U.S. agricultural land," was "the most spatially extensive drought to affect the country since the Dust Bowl of the 1930s," and gave the greatest summertime rainfall deficit to the Central Plains in 117 years to provide "a significant impact on the entire Central Plains' summer growing season."

Next is the severe to extreme drought over the southern United States and Mexico from 2010 to 2013 due to a strong La Niña that started in the summer of 2010, of which Texas

Brought to you by NOAA Central Library | Unauthenticated | Downloaded 08/13/24 07:18 PM UTC

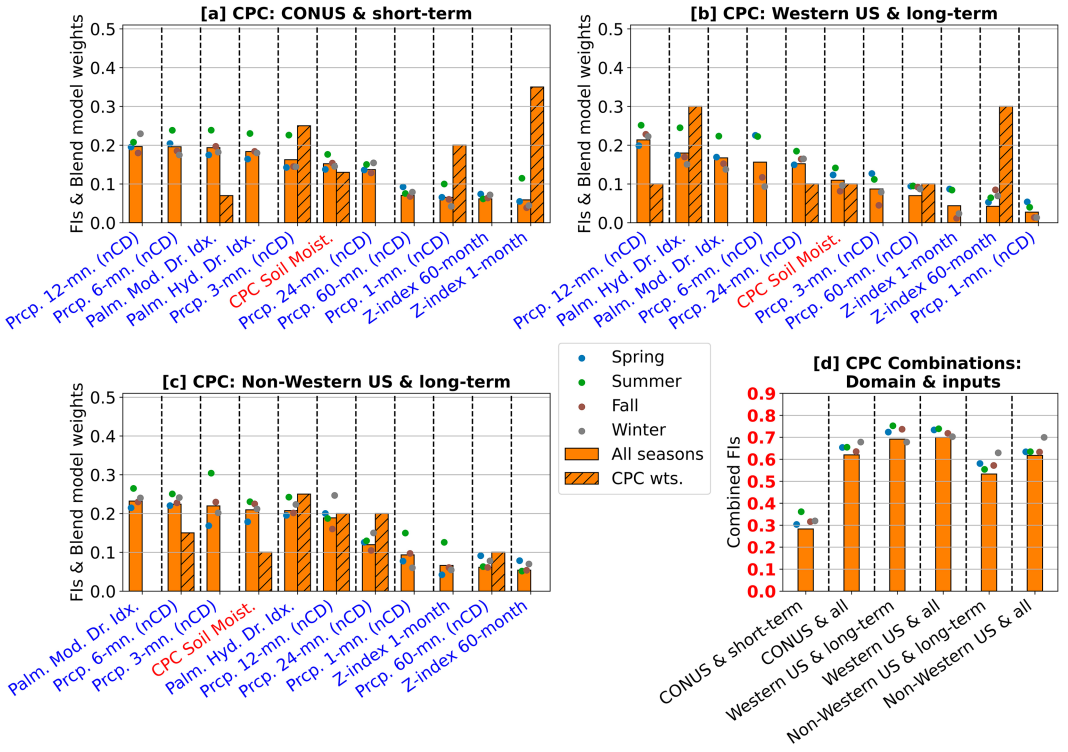



FIG. 3. (a)–(c) Individual FIs compared against weights from the CPC Blends and (d) combined FIs of the CPC Blends' input indicators. Titles in the former denote the combination of spatial domain and the relevant inputs, even though FIs for all 11 or 12 inputs are shown descend-sorted along the *x*-axis. Panel d shows the combined FIs for the relevant combinations of spatial domain and the inputs (for the latter, either the 5 or 6 relevant ones, or all 11 or 12). Red-colored *y*-axis tick values clarify a different range of those values than in (a)–(c). The colors of the *x*-axis tick labels in (a)–(c) correspond to two indicator subsets in Table 1, namely, observation based (blue) and model based (red).

suffered the worst effects during 2011 to form the worst Texas drought since 1895 (Pack 2011; Null 2023). The final drought event considered is the 2006–08 drought over the southeastern United States that was initiated by the 2005 La Niña in the eastern Pacific Ocean and joined by an unusually strong Bermuda high pressure system (Seager and Tzanova 2008; Seager et al. 2009; Null 2023). The initial dry period drought in 2006 mostly went away in the winter of 2006/07 before reemerging in April 2007.

## 3. Results

We first examine the FI values of only the input indicators used in the CPC and NDMC Blends, before considering our full set of 113 indicators and their subsets in subsequent subsections. Each reported FI value in the following subsections is the median value from among 101 values that result from different random seeds in the MI calculation (see section 2c). However, the vast majority of the 90% confidence interval ranges around these medians have values of less than 1%, and reach a maximum of near 3.9% for very few indicators during wintertime of some spatiotemporal drought events, making our following results and conclusions very robust.

### *a. Indicators used in the Blend products*

Here we compare our FI values that are calculated versus USDM maps (that represents both short- and long-term droughts) against the weights that are official values used in the linear models of drought categorization of the CPC and NDMC Blends (that are different for Short- and Long-Term). Note that while the NDMC Blend products are at the nClimGrid resolution, our analysis is done at the nClimDiv resolution (see section 2b and Table 2).

Results for CPC Blends are in Fig. 3 while those of NDMC Blends are similar and shown in supplemental Fig. S2. Figures 3a–3c show the FI values of each of the 11 or 12 inputs used in the Blends and arranged in descending order, compared against the Blends' weights. The order of importance of the FIs is very different from the weights and sometimes even contrasting. For example, Fig. 3a for the CPC Short-Term Blend shows that the highest and lowest weights for the 1-month *Z* index and the PMDI, respectively, are exactly opposite to the corresponding FIs being lowest and highest, respectively (see the third and the last *x*-axis tick labels). This holds even after considering variations in the range of the seasonal scatter dots around each FI bar. Figure 3b for the CPC Long-Term Blend over the Western region also depicts the

Brought to you by NOAA Central Library | Unauthenticated | Downloaded 08/13/24 07:18 PM UTC

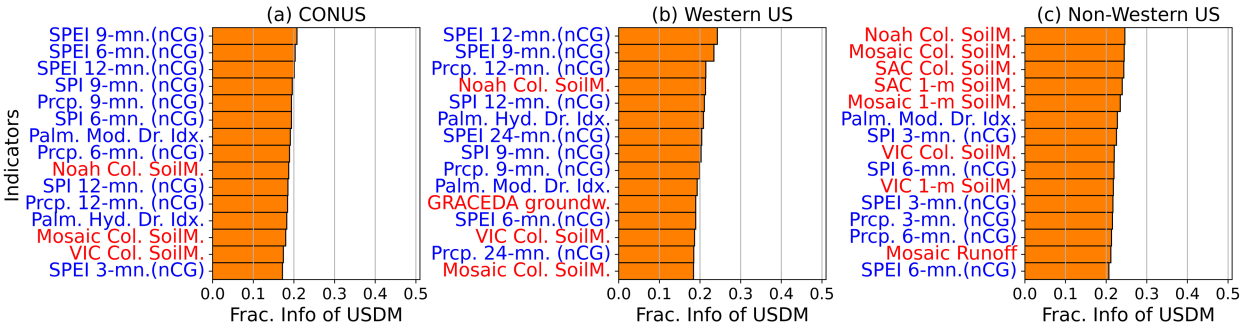



FIG. 4. Top 15 indicators per fractional information (FI) against USDM for each of the CPC regions as mentioned in the respective subplot title, when all data are considered independent of season. Sample size is the same among all the indicators in any subplot. The colors of the *y*-axis tick labels correspond to two indicator subsets in Table 1, namely, observation based (blue) and model based (red).

same behavior between the 12-month precipitation and the 60-month $Z$ index (the first and the next-to-last tick labels). The NDMC Blends also display this property for indicators that are equivalent to those in the CPC Blends (see section 2b, Table 2, and Fig. S2): the 1-month SPEI, 9-month SPI, 12-month SPI, and the 60-month SPEI in place of the 1-month $Z$ index, PMDI, 12-month precipitation, and the 60-month $Z$ index, respectively.

A noteworthy contrast of these FIs against the NADIIA ratings concerns the role of soil moisture for long-term drought. NADIIA has a single rating representing both short- and long-term droughts together, and which is consistently at the high end of 4–5 for all climate zones. However, the soil moisture weights in Figs. 3b and 3c (for Long-Term in Western and non-Western United States, respectively) (and Fig. S2b,c) are the lowest at 0.1.

Finally, over each CPC spatial domain, Fig. 3d shows FIs for the multivariate indicator of joint Blend inputs: these can be the 5 or 6 relevant to the domain, or all 11 or 12. These FIs are not yet near 100%, and the NDMC FIs improve by less than 10% from the CPC FIs (cf. Fig. 3d to Fig. S2d). This indicates that the official Blends products could substantially improve when adding additional indicator inputs. Specifically, the ~35% FI shown by the current five indicators in the NDMC Short-Term Blend over CONUS (Fig. S2d) increases to up to 70% when considering all 113 indicators over CONUS.

### *b. Top 15 among all 113 indicators*

Figure 4 shows the top 15 out of 113 indicators sorted by FI values for the entire CONUS and the CPC Western and non-Western U.S. regions. The presence of SPEIs, SPIs, precipitations, and modeled soil moistures in all three subplots conform to their high NADIIA ratings, except for medium rating of 3 for the soil moisture–related soil moisture anomaly indicator in the BWh and BSh Köppen climate zones that exist in the South and West regions. PMDI, PHDI (Figs. 4a,b), and groundwater (the GRACE DA groundwater as a red tick label in Fig. 4b) are also compatible with their medium to high ratings in almost all climate zones (note that we are comparing the PMDI FIs with the NADIIA ratings of the closely related PDSI). The only exception to this is a low PHDI rating of 2 for the Cfa zone that occurs in all regions and covers most of the South and almost all of Southeast.

Absent in NADIIA is runoff, which appears in the top FIs list over the non-Western United States (Mosaic runoff at the 14 position in Fig. 4c) and is a model-based indicator. This shows the value of our information theoretic analysis in providing knowledge that is complementary to NADIIA for drought monitoring, modeling, and forecasting efforts. The top two indicators in Figs. 4b and 4c also conform to expectations about the different hydroclimatic types in the Western and non-Western regions: the SPEIs in Fig. 4b represent a simple climatic water balance that captures the main impact of increased temperatures in the Western region on atmospheric water demand, while the soil moistures in Fig. 4c emphasize the role of the land surface elsewhere.

Figure 5 shows the FIs at the finer spatial scales of the USDM regions. The high FIs for runoff and soil moisture (among the red tick labels for model-based products) seen in the non-Western region in the previous Fig. 4c stems from their effect in the South, Southeast, and Northeast regions in Figs. 5d–f, respectively. These latter regions are also spatially coincident with the Cfa and Dfb humid climate zones (see section 2d). Some interesting differences exist between the time scales of highest FIs of relevant indicators across USDM regions. For example, precipitation, SPI, and SPEI are at time scales of 9–24 months in the top 15 in the USDM West region (Fig. 5a), but at time scales of 9–12 months in USDM High Plains (Fig. 5c), 6 months in USDM Southeast (Fig. 5e), and down to 3–6 months in the USDM Midwest, South, and Northeast regions (Figs. 5b,d,f). Figure 5f also shows the remote sensing–based IMERG precipitation showing up for the USDM Northeast (green tick label in Fig. 5f). Among soil water stores, the GRACE groundwater and some total column soil moistures FIs are in the top 15 in the USDM West (red tick labels in Fig. 5a), while both top 1-m and total column soil moistures for all NLDAS-2 and CPC products are seen for the USDM Midwest (Fig. 5b).

Figure 6 shows the top 15 FIs for each drought event in Table 3. This result reveals two indicators that are missing not only in Figs. 4 and 5, but also from NADIIA. The first is SWE as red tick labels for Northern Plains 2017 (Fig. 6a), Midwest/Central U.S. 2012 (Fig. 6c), and Southeast 2006–08 (Fig. 6e),

Brought to you by NOAA Central Library | Unauthenticated | Downloaded 08/13/24 07:18 PM UTC

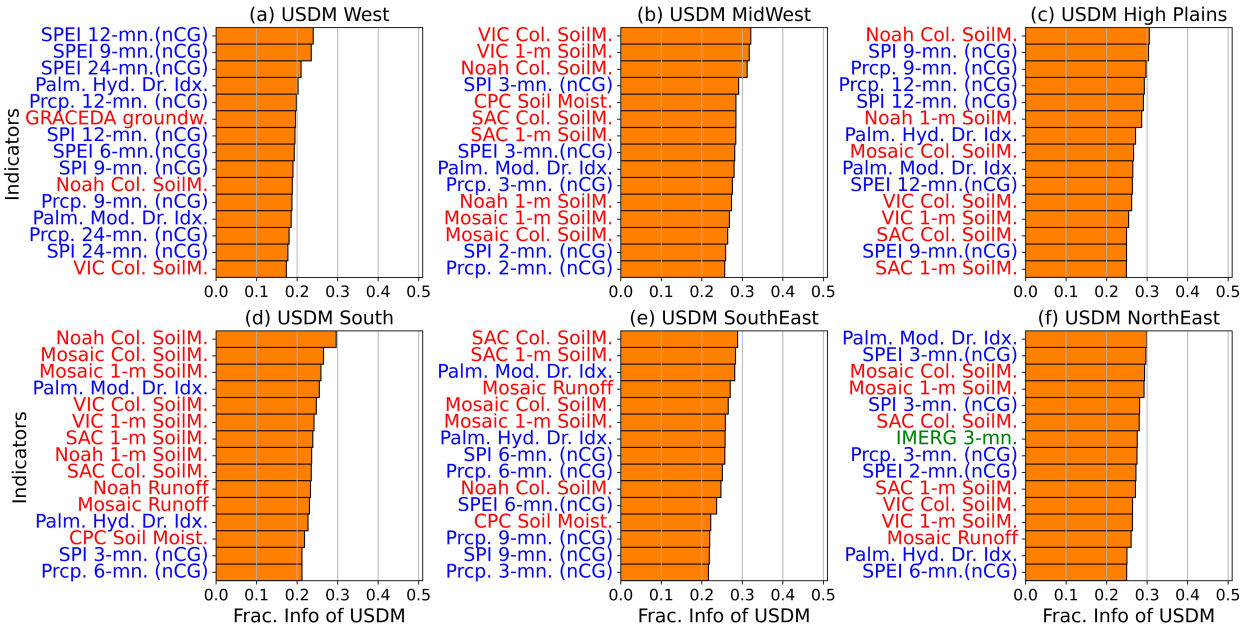



FIG. 5. As in Fig. 3, but for the USDM regions instead of the CPC regions. The colors of the *y*-axis tick labels correspond to the indicator subsets in Table 1, namely, observation based (blue), model based (red), and remote sensing based (green).

while the other is vegetation stress represented by VegDRI for Texas 2011 (green tick label in Fig. 6d). Figure 6e also shows EDDIs starting to appear for the Southeast 2006–08 event. Notably, the soil moisture FIs are not in the top 15 for the California 2012–17 event (Fig. 6b), and the absence of any land water stores shows its overwhelming domination by atmospheric dryness. Runoff is also conspicuously absent for all these drought events. Note that Figs. 6a–d reflect the preparation of samples for typical analytic and modeling methods wherein all (113) indicators have spatiotemporally coincident

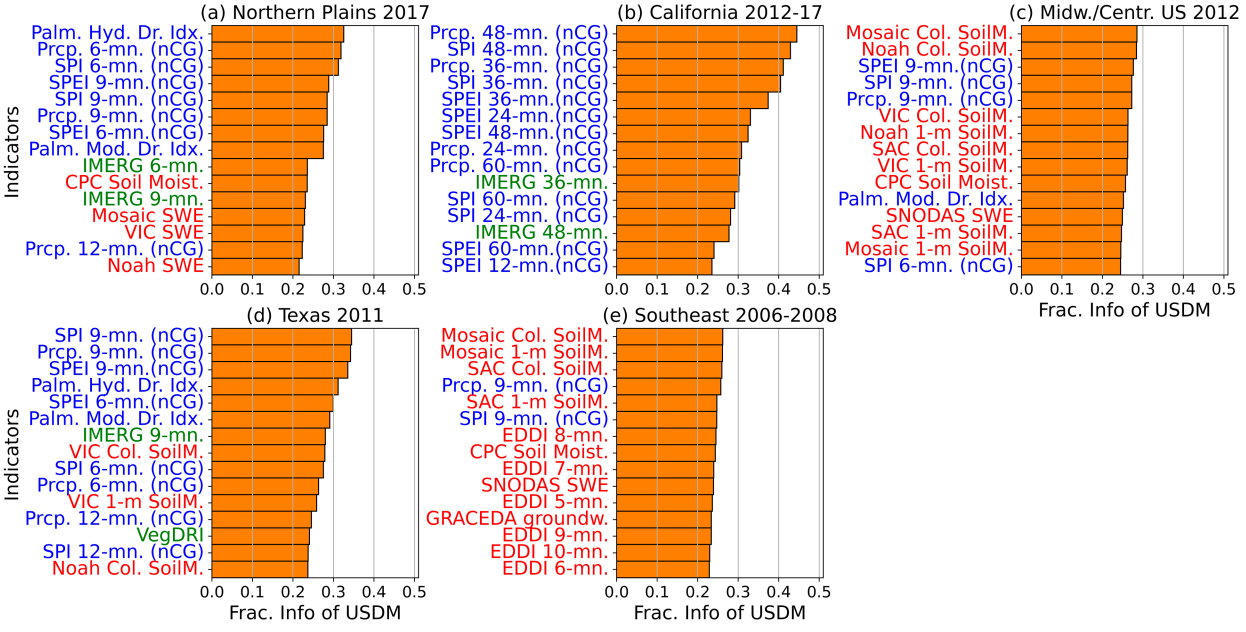



FIG. 6. (a)–(e) Top 15 indicators per fractional information (FI) against USDM for each event as mentioned in the respective panel title, when the data are considered independent of season. All indicators in any panel have the same sample size since only the samples having spatiotemporally coincident valid values across all (113) indicators are taken, except for (e) where the sample size of each indicator is independent of the validity of values of other indicators. The colors of the *y*-axis tick labels correspond to the indicator subsets in Table 1, namely, observation based (blue), model based (red), and remote sensing based (green).

Brought to you by NOAA Central Library | Unauthenticated | Downloaded 08/13/24 07:18 PM UTC

valid values to give the same sample size across all indicators. This would leave us with zero samples for the Southeast 2006–08 event (Fig. 6e), hence for that event, we instead considered the valid values for each indicator without considering the validity of corresponding values in the other indicators. This reflects some recent gap-agnostic modeling and prediction techniques in machine learning (e.g., Yatheendradas and Kumar 2022).

We now consider each season, starting with the spring season when snowmelt begins to translate into runoff. In contrast with Fig. 6, the top 15 indicators now include runoff for specific events like Southeast 2006–08 (Fig. S3n) and streamflows for the USDM South and Northeast regions (Figs. S3g,i). The 60-month $Z$ index is also shown in the top 15 and occurs for specific events like Northern Plains 2017 and California 2012–17 (Figs. S3j,k). VegDRI seen in Fig. 6d is now not in the top 15, and neither is GRACE DA groundwater for the Western United States (Fig. S3b) that was seen in Fig. 4b.

Moving onto summer season (Fig. 7) where snow is supposed to have completely or almost disappeared, the SWEs are surprisingly seen to play a prominent role especially for Northern Plains 2017 in Fig. 7j where the top six inputs are all SWEs, and except for California 2012–17 (Figs. 7j,l–n). This is likely be due to high temperatures melting all the snow into the water-scarce soil. Evaporation is seen in the top 15 from the VIC model for the Midwest/Central U.S. 2012 event (Fig. 7l). As in Spring, VegDRI is not in the top 15. For California 2012–17 (Fig. 7k), the topmost indicators having almost 80% FIs indicate high summertime predictability. All top 15 indicators for Southeast 2006–08 being model based (Fig. 7n) indicates the possibility of successful summertime forecasting of this event.

For the fall season, the snow products that were seen in Fig. 7l for summer have now disappeared from the top 15 for the Midwest/Central U.S. 2012 event (Fig. S4l). Similar to that seen in the transitional spring season, the fall season is also seen to list the 60-month $Z$ index for the Northern Plains 2017 and the California 2012–17 events (Figs. S4j,k). Finally considering winter, the role of snow is again counterintuitive as it was during summer but in a reverse manner: it is mostly not in the top 15 among these top indicators except for the Midwest/Central U.S. 2012 and Southeast 2006–08 events (Figs. S5l,n). This is likely due to the low winter temperatures permitting only a little melting of the existing large amounts of snow into the soil that is not water deficient anyway.

### c. *Patterns and trends across all 113 indicators*

Figure 8 shows the individual FIs for the example USDM West region. Before comparing across seasons, we first report on the trends seen for all seasons taken together (the orange bars) in Fig. 8 and supplemental Figs. S6–S17 for all spatial domains and events excluding Southeast 2006–08. These figures consider only those samples that have spatiotemporally coincident valid values across all the 113 indicators, while Figs. S18–S31 consider separate sample sizes for each of the indicators to exploit all available information so that Fig. S31 for Southeast 2006–08 is also included (see section 3b). The results from the two sets of figures are similar except for rare cases such as the example divergence in winter FI values at time scales of 24 months and higher for nClimGrid precipitations, SPIs, and SPEIs in the USDM High Plains region (supplemental Figs. S10a,b,f versus Figs. S23a,b,f). This demonstrates the robustness of these results across sample sizes, even when the sample size is lower for any season or years.

For any region and season, each indicator that has some range of time scales (precipitation, SPI, IMERG, SPEI, and EDDI in Figs. 8a, 8b, 8e, 8f, and 8i, respectively) mostly shows the highest FI values somewhere in the middle of that range. For example, Fig. 8f shows the 12-month time scale having the highest FI for SPEI when all the seasons are considered together (orange bars). Notable exceptions to this trend are the EDDIs for the USDM High Plains region (but not during summer; Fig. S10) and for the California 2012–17 event (Fig. S15) having the highest FIs at the coarsest 12-month time scale, indicating the potential of EDDIs to better capture such droughts if available at even coarser time scales. When comparing across USDM regions in the various figures, the USDM West region tends to have higher FIs at longer time scales (Fig. 8), for example, when compared against the USDM Midwest (Fig. S9).

For any region, season, and time scale, the FI value for precipitation is almost always similar to that for SPI, indicating the redundancy between them for capturing drought (e.g., Figs. 8a,b). Also, note from Fig. 8i that the FI values for the 4-, 8-, and 12-week EDDIs are almost the same as expected to those for the 1-, 2-, and 3-month EDDIs, respectively, because of the comparison time periods being almost the same. Similarly, keep in mind that the FIs for the USDM West region are expectedly similar to that of the CPC's Western U.S. region (Fig. S7) because these regions are mostly the same (Fig. 1). Finally, note that indicators like evaporation, air temperature and SWE are not present in the NADIIA ratings, so that the information from our FI values is invaluable for the drought community.

#### 1) Data patterns independent of season

The IMERG FIs for the USDM West region (Fig. 8e) give approximately only half the information provided by the precipitation FIs (Fig. 8a). However, the FIs for IMERG in the non-Western U.S. region are close to those of the observed precipitation (Figs. S8a,e). This indicates that the IMERG precipitation is a potential reliable substitute for the observed nClimGrid precipitation in the Eastern but not the Western United States. Except for the USDM West region and the California 2012–17 event (Fig. 8, Fig. S15), the average FIs over the subyearly time scales (12 months or less) for precipitation, SPI, and SPEI are higher than those over the time scales greater than yearly (Figs.8a,b,f and Figs. S15a,b,f). Observed average and maximum air temperatures give low FI values, and surprisingly, the FIs for modeled evaporations are not high for the USDM West region (Fig. 8g).

The FI for the ESA CCI remotely sensed soil moisture product is near-zero in the Western United States and a small value of near 5% in the Eastern United States (Fig. 8j, Fig. S8j). In all the USDM regions and events, the FIs for the modeled soil moistures (except GRACE DA) are mostly seen to be in the 20%–30% range (Figs. S9j–S17j and S31j,

Brought to you by NOAA Central Library | Unauthenticated | Downloaded 08/13/24 07:18 PM UTC

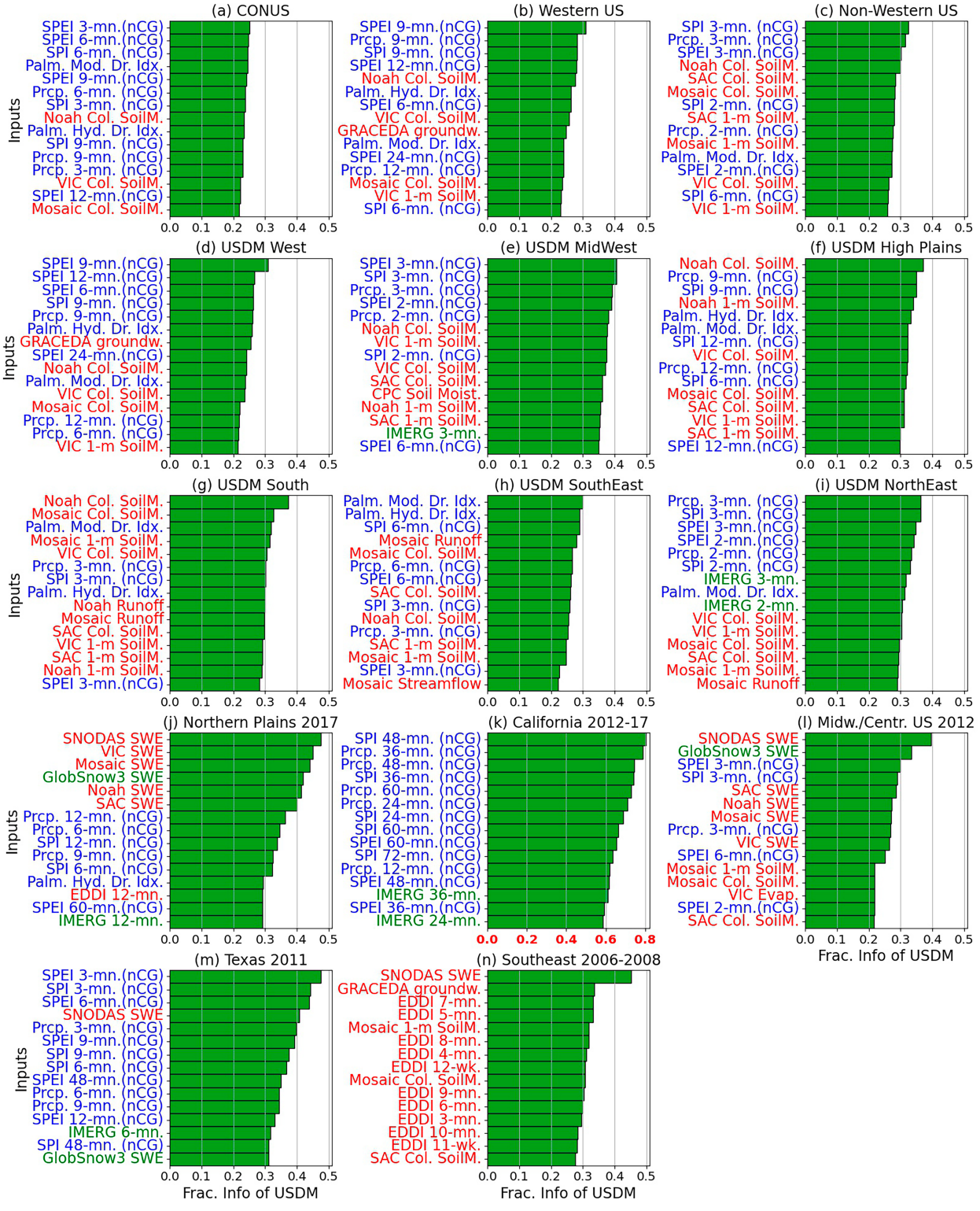



FIG. 7. (a)–(n) Top 15 indicators per fractional information (FI) against USDM for each spatial domain or event as mentioned in the subplot title, when the data of only the summer season are considered. All indicators in any subplot have the same sample size since only the samples having spatiotemporally coincident valid values across all (113) indicators are taken, except for (n) where the sample size of each indicator is taken independent of the validity of values of other indicators. The colors of the *y*-axis tick labels correspond to the indicator subsets in Table 1, namely, observation based (blue), model based (red), and remote sensing based (green).

Brought to you by NOAA Central Library | Unauthenticated | Downloaded 08/13/24 07:18 PM UTC

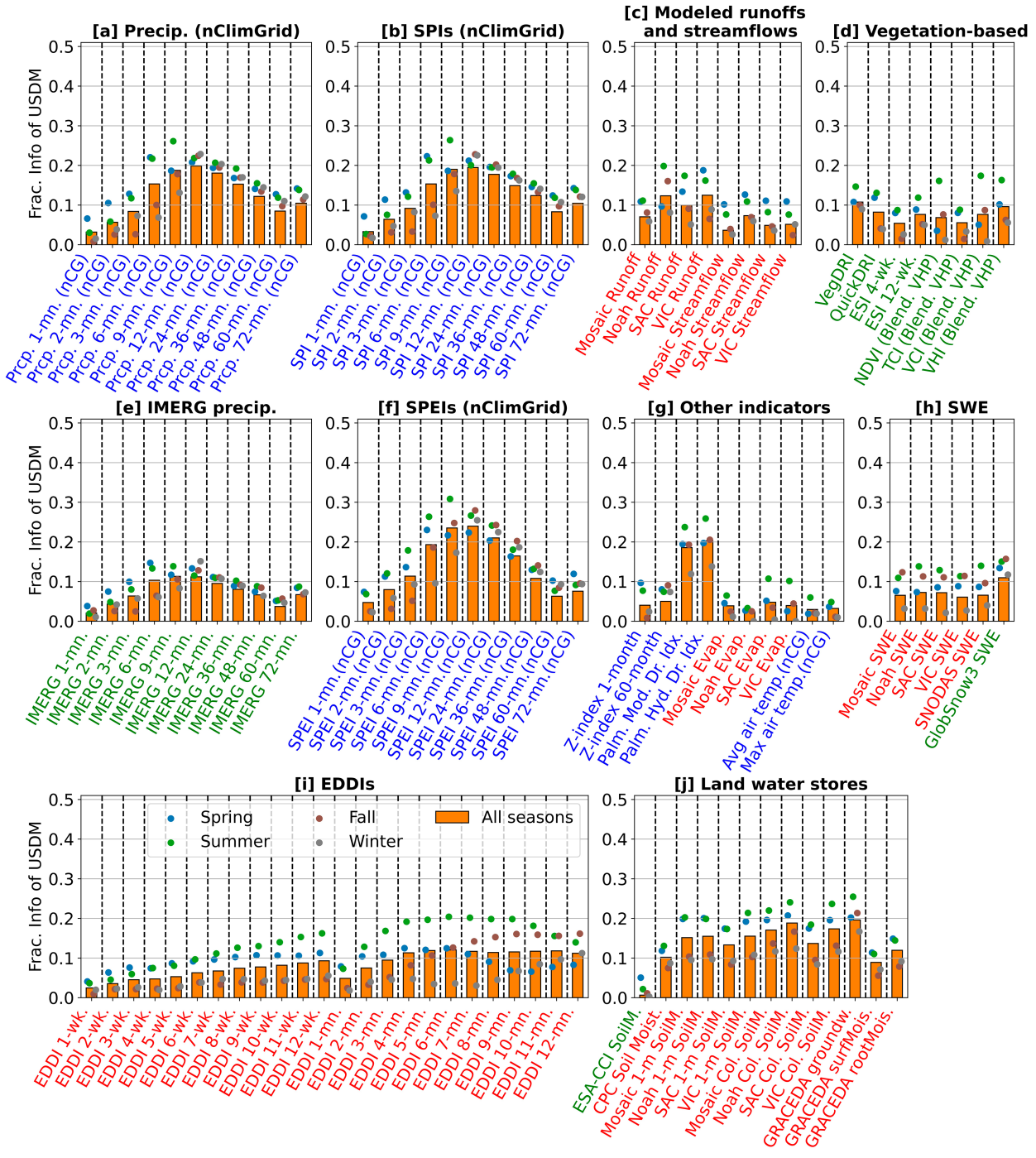



FIG. 8. FIs for indicators grouped into subplots by indicator type for the example USDM West region. All indicators have the same sample size since only the samples having spatiotemporally coincident valid values across all (113) indicators are taken. The colors of the *x*-axis tick labels correspond to the indicator subsets in Table 1, namely, observation based (blue), model based (red), and remote sensing based (green).

versus Fig. 8j), except for lower ranges in the USDM West region and the California 2012–17 event. The SWEs have around 10% FI in most USDM regions but have near-zero values except for the SNODAS SWE in the USDM South and Southeast regions. These latter regions by extension mean the Cfa or humid subtropical climate zone (refer section 2d) which gets very little snowfall. However, NLDAS-2 SWEs have higher FI of approximately 20% for the Northern Plains 2017 and the Midwest/Central U.S. 2012 events (Figs. S14h and S16h, respectively).

Brought to you by NOAA Central Library | Unauthenticated | Downloaded 08/13/24 07:18 PM UTC

The modeled runoffs consistently capture slightly more USDM drought information than the modeled streamflows, with the notable exception of the California 2012–17 event where it is the opposite (panel c in Figs. 8 and S6–S17). This California 2012–17 drought event appears to be distinct from the others in operating at longer time scales: the precipitation and SPEI peaking at 36–48 months, and the QuickDRI and 4-week ESI being near zero. The latter two indicators are part of the blended-VHP products among which the VHI or TCI give the highest FI.

#### 2) Patterns across seasons

Panels a, b, and f in Fig. 8 and Figs. S9–S11 show that for most USDM regions, the highest interseasonal variations in FI values of nClimGrid precipitation, SPI, and SPEI occur at mainly the finer time scales, with summer (winter) typically showing the highest (lowest) FIs at these time scales. But Figs. S12 and S13 respectively show the Southeast (and so the Cfa zone or humid subtropical climate) and Northeast (and Dfb zone or the humid continental mild summer, wet all year) having the highest variations occurring at the coarser time scales for these indicators with winter now actually showing the corresponding highest FIs, even though the finer time scales do show significant interseasonal variations. For all events, the highest interseasonal variations occur at the coarser time scales for these indicators whereas the specific season showing the highest FIs at these time scales varies.

The interseasonal variations in FI values of runoff and streamflow mostly approach the magnitudes of FIs for the West and Midwest regions, and mostly are greater than them for the events (Fig. 8c and Figs. S9c–S17c and S31c). NADIIA assigns the highest rating of 5 for streamflow for drought overall in the Cfa climate zone. This contrasts with the FI value of less than 16% in fall season streamflows for the corresponding USDM South region (Fig. S11c).

### *d. Combined FIs of indicators*

#### 1) Considering all the indicators of each subset

Figures 9a–c show the combined FIs of the different subsets of drought indicators in Table 1: all 113, primarily remote sensing based, and primarily model based. Since precipitation is the main forcing for a hydrological phenomenon like drought, we added one more subset of indicators in Fig. 9d by adding nClimGrid precipitations to the indicators in Fig. 9c. Note that the NLDAS-2 model outputs are obtained using observed precipitation as one of the forcings, and the NLDAS-2 dataset includes precipitation as one of its variables. This means that the FIs in Fig. 9d will be similar to that obtained when the nClimGrid precipitations in this subset are substituted by the corresponding NLDAS-2 precipitation variables. The obtained combined FIs are robust because there is consistency between the numbers in Figs. 9b–d (wherein the spatiotemporally coincident valid values of all 113 indicators are considered together) with the corresponding ones in Fig. S32 (wherein the validity is considered only across indicators in each subset).

The first three bars for the CPC regions in Fig. 9a each have only 5%–10% more FI than the corresponding bars that use all NDMC inputs (Fig. S2d). This indicates that a large number of indicators together might not necessarily capture significantly extra information of USDM drought. Rather, carefully selecting small sets of indicators like those in the NDMC Blends, while additionally ensuring very little interacting or redundant information among the indicators, can capture almost as much combined information as the large set. Additionally, it is possible for subset/s of indicators to actually have more combined information than the full set if the contradicting USDM drought information (the negative interactions that can actually reduce the captured combined information) between the subset indicators is eliminated.

Such negative interactions can result in the combined FIs not reaching 100%, other reasons for which include our not considering differences over time of either the existing indicators to give new indicators (see section 2e), or of the USDM maps since the map authors ensure some level of consistency with the previous week's map. Also, our information theoretic analysis does not capture the USDM authors' skill and experience. The FIs for the USDM regions and events in Fig. 9a are noticeably lower (<60%) in winter for the Midwest, in winter and fall for the Northern Plains 2017 event, and in fall for the Midwest/Central U.S. 2012 event. On the other hand, the California 2012–17 event reached a high FI of 90% during summer when the drought peaked.

Finally, Figs. 9b–d show that the FIs for all seasons considered together (orange) have dropped by only up to about 10%, 15%, and 5%, respectively, from corresponding numbers in Fig. 9a. This is encouraging both for future efforts by the remote sensing and modeling communities in recreating similar drought monitors, and for the forecasting community since the FIs in Fig. 9d form the upper limits for retrospective prediction accuracy that in turn are the theoretically attainable upper limits for forecast accuracy.

#### 2) Top 15 indicators of each subset

We calculated combined FIs for the top 15 indicators from each subset of indicators considered in the previous section 3d(1), where the sorting order to select the top indicators comes from section 3b. The combined FIs mostly reduce by up to 20%, 12%, 11%, and 11%, respectively, from Figs. 9a–d and 10a–d. Following the discussion in section 3d(1), these reduction percentages in panels c and d reinforce the possibility that a judicious selection of indicators from among the top ones can enable effective drought monitoring and forecasting by both the remote sensing and modeling communities. The combined FI is seen to actually increase (due to possible elimination of contrasting information between indicators) for the Western region and the California 2012–17 event in panel a, the California 2012–17 event with about 5% gain in panel b, and the Northern Plains 2017 event by 10% gain in panels c and d.

### *e. Sensitivity to statistical distributions of SPI and SPEI*

As mentioned in section 2b, we now briefly report on the sensitivity of our results to the distributions of the SPI and

Brought to you by NOAA Central Library | Unauthenticated | Downloaded 08/13/24 07:18 PM UTC

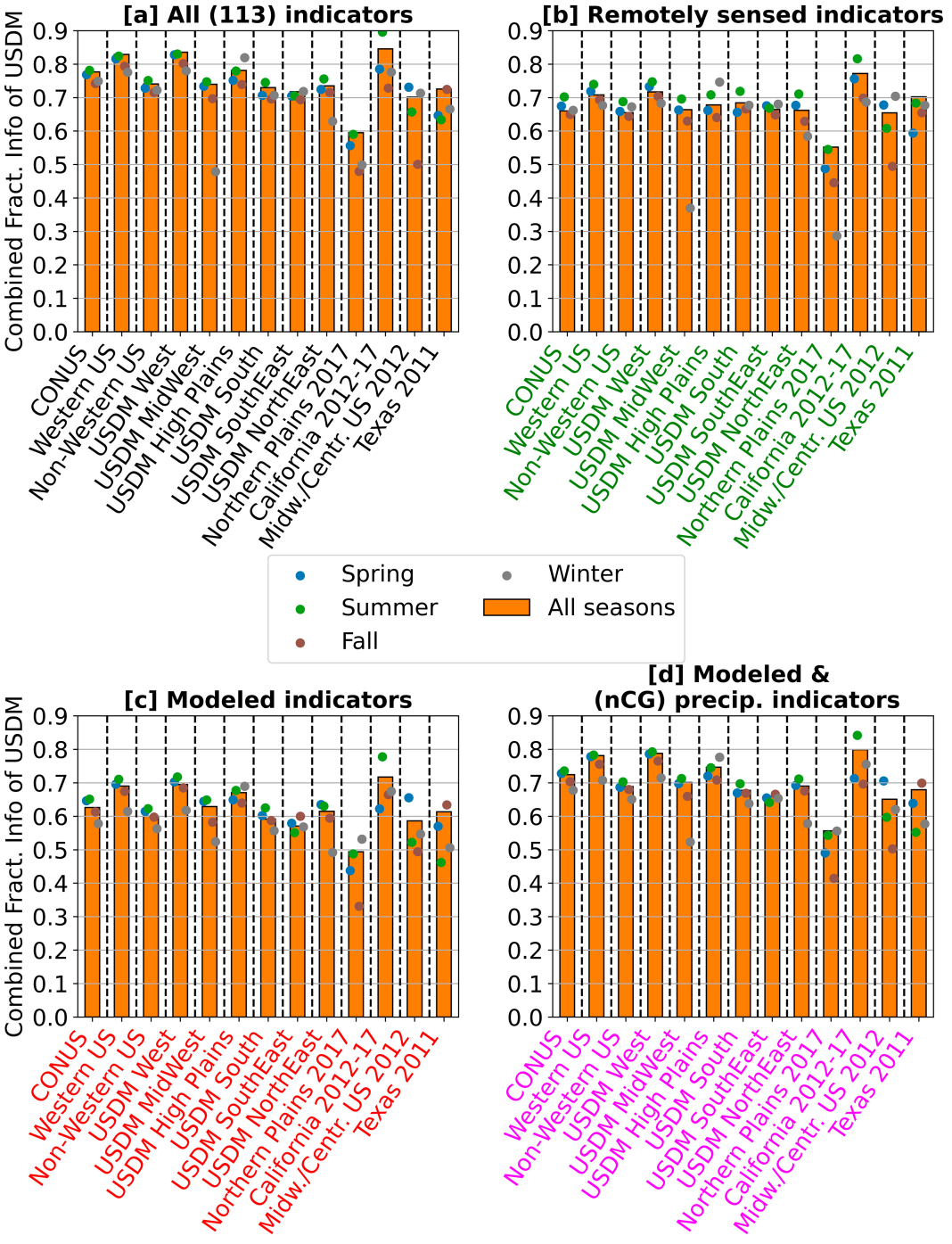



FIG. 9. Combined FI for each subset of indicators, spatial domain/event and season. Panels have respective subsets of (a) all 113 indicators, (b) remotely sensed, (c) modeled, and (d) modeled plus nClimGrid precipitations. For any spatial domain (*x*-axis tick label), the sample size is the same across all subplots since only the samples having spatio-temporally coincident valid values across all (113) indicators are taken. The colors of the *x*-axis tick labels correspond to the different indicator subsets in Table 1, namely, observation based (blue), model based (red), and remote sensing based (green), except for (d) wherein the labels have a magenta color (red + blue) to reflect the combination of observation-based nCG precipitation and model-based indicators.

Brought to you by NOAA Central Library | Unauthenticated | Downloaded 08/13/24 07:18 PM UTC

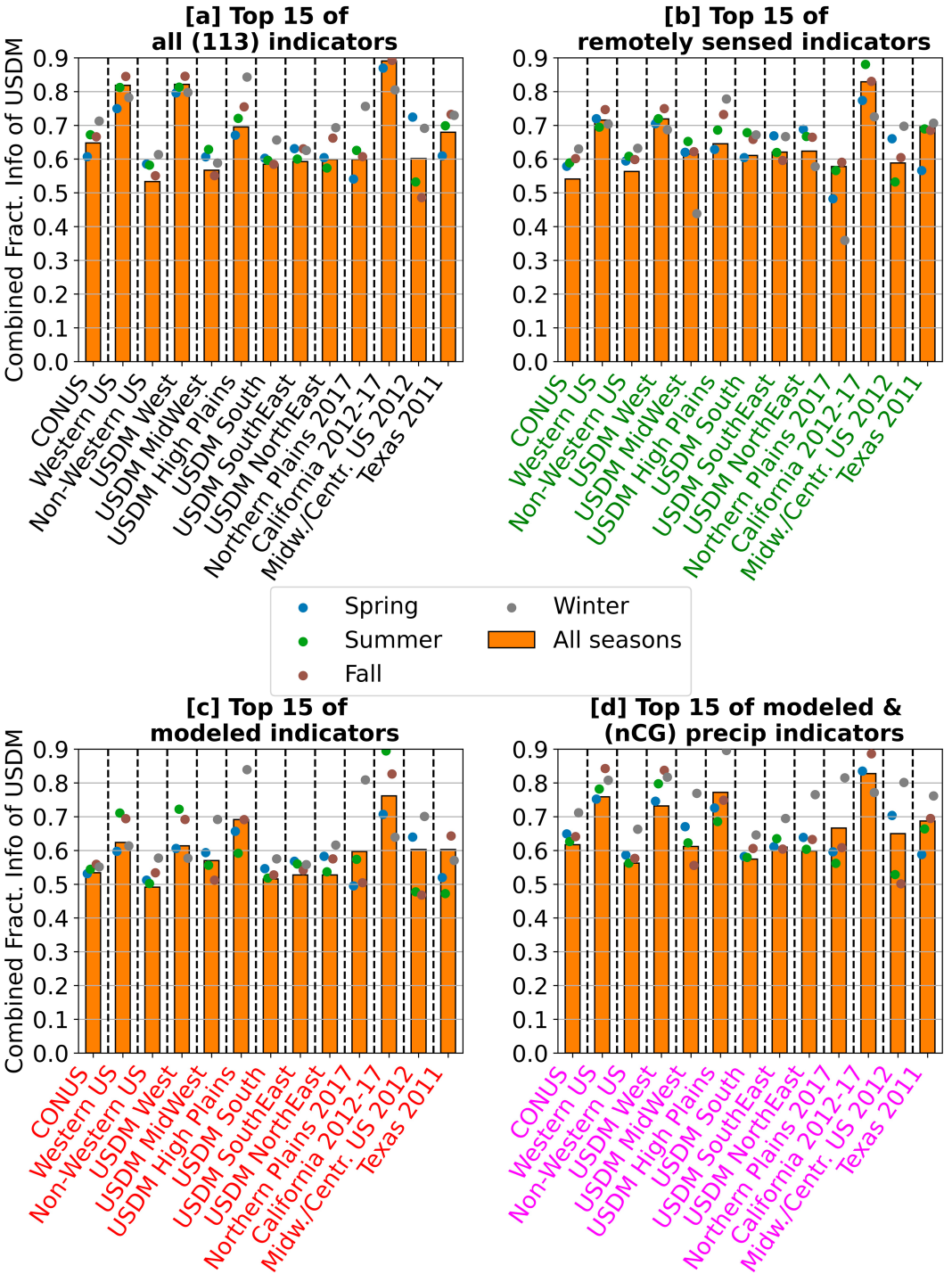



FIG. 10. Combined FI for top 15 indicators (per individual FI) from each subset of indicators for each spatial domain/event and season. Panels correspond to respective subsets of (a) all 113 indicators, (b) remotely sensed, (c) modeled, and (d) modeled plus nClimGrid precipitations. For any spatial domain (*x*-axis tick label), the sample size is the same across all subplots since only the samples having spatiotemporally coincident valid values across all (113) indicators are taken. The colors of the *x*-axis tick labels correspond to the different indicator subsets in Table 1, namely, observation based (blue), model based (red), and remote sensing based (green), except for (d) wherein the labels have magenta color (red + blue) to reflect combination of observation-based nCG precipitation and model-based indicators.

Brought to you by NOAA Central Library | Unauthenticated | Downloaded 08/13/24 07:18 PM UTC

SPEI indicators. Our reported results till now use the gamma distribution for SPIs and Pearson for SPEIs (we refer to this as the "baseline"). For the sensitivity of the combined FIs, we compare this baseline against the other three pairs: Pearson for SPEIs with gamma for SPIs, then gamma for both indicators, and finally Pearson for both. We found the maximum FI difference for any of these pairs with the corresponding baseline to be a negligible 1.2%.

Next we compare the baseline individual FIs against the corresponding FIs from the other distribution (Pearson for SPEI and gamma for SPI). Assuming that differences greater than 5% are significant, we saw some significant differences when the samples consisted of spatiotemporally coincident valid values across all 113 indicators. For the USDM regions, only three such cases arose and during winter: a difference of 6.1% for 2-month SPEI in the Midwest, and 15.8% and 5.3% for 72- and 60-month SPI, respectively, in the Northeast. However, for events, we saw many more and much higher significant differences for most of them with the maximum reaching 20.5% for 72-month SPEI during the Northern Plains 2017 event, 10.7% for 60-month SPEI during California 2012–17, 6.1% for Midwest/Central U.S. 2012, 7% for Texas 2011, and 5.4% for Southeast 2006–08.

## 4. Discussion and conclusions

Information on the relative importance of drought indicators by location and season is important to stakeholders. To objectively calculate such information for drought—as represented by the U.S. Drought Monitor (USDM)—this study uses metrics from the well-established and model-independent technique of information theory on a subjectively selected list of 113 indicators. There is some overlap between the indicators in our study and those officially used by USDM authors in creating the USDM maps, but there are also indicators that are present in one and not in the other. We calculated the mutual information between any indicator/s and the USDM, and then normalized it by the entropy of USDM to give the fractional information (FI) metric that enables comparison across spatial regions and time scales. We have reported results at the scales of USDM hydrologic regions, seasons, and drought events. Further, we envision these results playing an important role as a reference and as an upper limit on the predictability obtained with other techniques having models with constraints imposed by their respective model structures.

We compared these values against other sources including the drought representation effectiveness ratings in the North America Drought Indices and Indicators Assessment survey (NADIIA). The NADIIA ratings are arguably a subjective community consensus, and not comprehensive in the list of indicators rated or the multiplicity of time scales at which relevant indicators are rated. As shown above, our technique can provide FI values for indicators that are absent in other sources like these NADIIA ratings, thus providing complementary and objective knowledge (e.g., runoff, SWE, QuickDRI, evaporation, and air temperature). Additionally, note that our individual indicator FIs are objective absolute values with the maximum seen to be just below 50% and not 100%, while the corresponding NADIIA ratings attain the maximum value of 5 so that they are likely only relative ratings. Because of this, we also recast our results using a relative approach of partitioning the FIs among five consecutive ranges so that the highest-values range will also contain some FI values, to enable a better comparison against NADIIA.

Hence, we are now able to answer our first study question in section 1:

1) These FIs are an invaluable resource both as an objective reference and as a complementary source of information for indicators not available from other sources.

Convergence of evidence for any indicator in terms of both individual FI values and NADIIA ratings being on the higher end adds confidence to their importance in representing drought, for example, indicators like SPEI, SPI, PMDI/PDSI, and PHDI, or their specific time scales. On the other hand, a divergence of evidence between our FIs and other sources suggests the need for further investigation and/or better data sources for a particular indicator. For example, if using only remotely sensed products, an alternative to the ESA CCI remotely sensed soil moisture product is needed for Western United States, where we obtain near-zero FI values. The Soil Moisture Active Passive (SMAP) mission may fill this role in the near future, but we were unable to use it in this study because its small period of record is insufficient for calculating percentiles.

Looking at specific indicators and time scales revealed important drought precursors, such as through snowmelt into water-scarce soil. It also highlighted expected hydroclimatic differences such as temperature/ET effects as reflected in SPEI for Western regions and soil moisture in non-Western regions.

Hence, we are able to provide the following answer to the second study question:

2) The FIs yielded process insights about dominating hydrological mechanisms and hydroclimate types, but also about potential objective drought assessment.

As noted in the introduction, the FI calculation between any multidimensional indicator and the USDM provides an "upper bound" on the possible accuracy obtainable using that set of indicator inputs in reproducing the USDM maps using any model-based estimation techniques (e.g., machine learning using convolutional neural networks or random forests). As our results show, the full 113-indicator set is capable of representing up to 90% of the FI in the USDM. The selected subsets of "top 15 indicators" or "model based" or "remotely sensed" are able to capture much of the same information—typically 0.6–0.8 versus up to 0.9 with the full set.

Thus, we can answer the remaining two study questions:

3) The high (0.6–0.7) combined FIs of the model-based indicators or its subset of 15 top indicators do indeed show promise for sufficiently accurate drought forecasts.
4) The remotely sensed indicators by themselves can be used for effective drought monitoring and even in in situ data scarce locations, as shown by their combined FI values of 0.7–0.8.

Brought to you by NOAA Central Library | Unauthenticated | Downloaded 08/13/24 07:18 PM UTC

These conclusions helped motivate a follow-on paper where we will demonstrate an objective drought estimation methodology using a trained random forest model.

Our study has not considered the uncertainty in the results from interpolation to other spatiotemporal resolutions and scales besides the climate polygon spatial resolution, the weekly time resolution and the spatiotemporal scales considered here. We investigated the uncertainty of our results to the statistical distributions of SPI and SPEI in section 3e to find that our conclusions hold almost all the time in the CPC or USDM regions and most of the time during the considered drought events. The mutual information (MI) technique itself has a little uncertainty stemming from a random seed parameter, and the related maximum uncertainty of 3.9% seen in the 90% confidence interval ranges of FIs around the median FI values show their robustness and hence of that the associated conclusions.

Finally, note that this type of work is resource intensive in terms of computational resources and time. However, we welcome further work on this topic by other researchers for analyzing more indicators or at different spatial resolutions. In this aspect, considering new indicators formed from considering differences over time of currently existing indicators or the USDM maps have the potential to be productive in extracting more drought information that is not captured otherwise.

*Acknowledgments.* This work was financially supported by NOAA's National Integrated Drought Information System (NIDIS) and Modeling, Analysis, Predictions, and Projections (MAPP) programs, both of which programs are within the NOAA Climate Program Office. Resources supporting this work were provided by the NASA High-End Computing (HEC) Program through the NASA Center for Climate Simulation (NCCS) at Goddard Space Flight Center. The NLDAS-2 and GRACE DA data used in this effort were acquired as part of the activities of NASA's Science Mission Directorate, and are archived and distributed by the Goddard Earth Sciences (GES) Data and Information Services Center (DISC). The producers and distributors of all the 113 drought indicators used in this study are sincerely thanked for their efforts.

*Data availability statement.* Codes and their generated data for this study (including the "analysis ready" database of 113 drought indicators) will be uploaded on https://zenodo.org/record/8259997.

## APPENDIX

### Some Background on Information Theory

For easier understanding, we explain in terms of a discrete variable having $N$ equally likely outcomes. The information then required in terms of the minimum number of binary questions to determine the variable's true outcome is (by visualizing it as a binary decision tree):

$$I = \log_2 N = -\log_2(1/N), \tag{A1}$$

where $1/N$ is the probability of hitting the true outcome after a single question. In general, when the outcomes are not equally likely, the information needed to get outcome $n$ where $n$ ranges from 1 to $N$ and $P_n$ is its probability is

$$I_n = -\log_2 P_n. \tag{A2}$$

The information then needed to get any outcome from these $N$ true outcomes is the expected value:

$$H = E\{I_n\} = -\sum_{n=1}^{N} P_n \log_2 P_n. \tag{A3}$$

Dropping the logarithm base, the formal definition of entropy for a random variable $X$ with $N$ possible values $x_n$ is

$$H(X) = -\sum_{n=1}^{N} P(x_n)\log P(x_n). \tag{A4}$$

This $H(X)$ is also a measure of uncertainty, and is maximum when all the $x_n$ are equally likely as a uniform distribution:

$$H_{\max}(X) = \log N. \tag{A5}$$

Its minimum value is $H_{\min}(X) = 0$ when all outcomes except one have zero probability denoting absolute certainty for that single outcome.

For multiple variables that form a multidimensional variable similar to multidimensional indicators considered in our study, Eq. (A4) then becomes a joint entropy formula:

$$H(\text{X1, X2, X3, } \ldots) = -\sum_i \sum_j \sum_k \ldots P(x_i, x_j, x_k, \ldots) \times \log P(x_i, x_j, x_k, \ldots), \tag{A6}$$

where $x_i$, $x_j$, $x_k$ represent outcomes from the respective discrete $I$, $J$, $K$ number of outcomes of X1, X2, X3, respectively.

Back to a single variable $X$, if we now considering a second variable $Y$ (similar to the USDM indicator in our study) with representative outcome $y_z$, then the resultant residual uncertainty called the conditional entropy of $X$ given $Y$ is

$$H(X|Y) = -\sum_n \sum_z P(x_n, y_z)\log P(x_n|y_z). \tag{A7}$$

The information complementary to this conditional entropy is what $X$ actually has in common with $Y$ and is called the mutual information (MI):

$$I(X; Y) = H(X) - H(X|Y) = -\sum_n \sum_z P(x_n, y_z)\log[P(x_n)/P(x_n|y_z)]. \tag{A8}$$

Here, $I(X; Y)$ will be equal to $I(Y; X)$ always. Instead of the residual entropy, we can use the joint entropy $H(X, Y)$ of $X$ and $Y$ adapted from Eq. (A6) to give another formulation:

$$I(X; Y) = H(X) + H(Y) - H(X, Y). \tag{A9}$$

Replacing the $X$ in Eq. (A8) by a multidimensional variable gives the following:

Brought to you by NOAA Central Library | Unauthenticated | Downloaded 08/13/24 07:18 PM UTC

$$I(\mathrm{X1},\ \mathrm{X2},\ \mathrm{X3},\ \ldots;\ Y) = -\sum_i \sum_j \sum_k \ldots \sum_z P(x_i, x_j, x_k, \ldots, y_z) \times \log P(x_i, x_j, x_k, \ldots | y_z). \quad \text{(A10)}$$

The MI from Eqs. (A8) and (A10) can be divided by $H(Y)$ to get the FI of $Y$ captured by $X$ or its multidimensional version, and this FI is used in our study. FI values range from 0% to 100% (or from $X$ capturing none to all the variation in $Y$).

This MI equation between discrete variables is inherently accurate and straightforwardly considers the relative frequencies for each combination of those variables. However, for MI between two continuous or real-valued variables, the legacy method of initially lumping into equal-width bins can cause imbalanced sampling (i.e., different numbers of samples across bins) as well as trade-off problems between the bin resolution and adequate sampling. The latter means that an accurate estimation requiring a good resolution (or smaller-width bins) can assign an insufficient number of samples to the bins.

Instead of equal widths, balanced sampling can be achieved by binning into equal frequencies (e.g., Darbellay and Vajda 1999) to result in bins of unequal width, and then possibly considering some inverse function of the bin widths for the MI estimator. However, this can still give undesirable resolutions for some bins, and is also subject to the uncertainty stemming from the exact placement of the bin edges. Kraskov et al. (2004) overcame these difficulties by instead using statistics of the distances between the data points and their nearest neighbors. Ross (2014) extended that work to derive an MI estimator between a continuous and a discrete variable and demonstrated it to be much more reliable than a binning approach.

Another factor to consider in this study is that we did not include any inputs that are differences over time of the considered 113 inputs (see section 2e), and such temporal changes can possibly provide more useful information. A related concept that we did not consider in this study is the information captured of the temporal differences between drought categories in consecutive USDM maps, since the authors of the USDM maps might prefer some level of explicit compatibility with the previous week's USDM map. Last, it is to be noted that the USDM map creation process is not automated, meaning that the authors' skill and experience can play an uncaptured role by our information theoretic analysis, and which is manifested by combined FIs being not near 100%.

## REFERENCES


Amorocho, J., and B. Espildora, 1973: Entropy in the assessment of uncertainty in hydrologic systems and models. *Water Resour. Res.*, **9**, 1511–1522, https://doi.org/10.1029/WR009i006p01511.

Anderson, M. C., J. M. Norman, J. R. Mecikalski, J. A. Otkin, and W. P. Kustas, 2007: A climatological study of evapotranspiration and moisture stress across the continental United States based on thermal remote sensing: 2. Surface moisture climatology. *J. Geophys. Res.*, **112**, D11112, https://doi.org/10.1029/2006JD007507.

Beck, H. E., N. E. Zimmermann, T. R. McVicar, N. Vergopolan, A. Berg, and E. F. Wood, 2018: Present and future Köppen-Geiger climate classification maps at 1-km resolution. *Sci. Data*, **5**, 180214, https://doi.org/10.1038/sdata.2018.214.

Beguería, S., S. M. Vicente-Serrano, F. Reig, and B. Latorre, 2014: Standardized Precipitation Evapotranspiration Index (SPEI) revisited: Parameter fitting, evapotranspiration models, tools, datasets and drought monitoring. *Int. J. Climatol.*, **34**, 3001–3023, https://doi.org/10.1002/joc.3887.

Bond, N. A., M. F. Cronin, H. Freeland, and N. Mantua, 2015: Causes and impacts of the 2014 warm anomaly in the NE Pacific. *Geophys. Res. Lett.*, **42**, 3414–3420, https://doi.org/10.1002/2015GL063306.

Brown, J. F., B. D. Wardlow, T. Tadesse, M. J. Hayes, and B. C. Reed, 2008: The Vegetation Drought Response Index (VegDRI): A new integrated approach for monitoring drought stress in vegetation. *GISci. Remote Sens.*, **45**, 16–46, https://doi.org/10.2747/1548-1603.45.1.16.

Caselton, W. F., and T. Husain, 1980: Hydrologic networks: Information transmission. *J. Water Resour. Plann. Manage. Div.*, **106**, 503–520, https://doi.org/10.1061/JWRDDC.0000170.

Cheng, W.-L., Y.-C. Kuo, P.-L. Lin, K.-H. Chang, Y.-S. Chen, T.-M. Lin, and R. Huang, 2004: Revised air quality index derived from an entropy function. *Atmos. Environ.*, **38**, 383–391, https://doi.org/10.1016/j.atmosenv.2003.10.006.

Critchfield, H. J., 1974: *General Climatology*. 3rd ed. Prentice-Hall Inc., 446 pp.

Dalezios, N. R., and P. A. Tyraskis, 1989: Maximum entropy spectra for regional precipitation analysis and forecasting. *J. Hydrol.*, **109**, 25–42, https://doi.org/10.1016/0022-1694(89)90004-8.

Darbellay, G. A., and I. Vajda, 1999: Estimation of the information by an adaptive partitioning of the observation space. *IEEE Trans. Inf. Theory*, **45**, 1315–1321, https://doi.org/10.1109/18.761290.

Dorigo, W., and Coauthors, 2017: ESA CCI soil moisture for improved Earth system understanding: State-of-the art and future directions. *Remote Sens. Environ.*, **203**, 185–215, https://doi.org/10.1016/j.rse.2017.07.001.

Downey, M., 2020: Flash Drought Montana 2017. National Integrated Drought Information System, https://www.youtube.com/watch?v=afWwhCNdP24&list=PLmhxKH4OH8KL84RwVzD–lMcwcdumHcPH&index=4.

Drought.gov, 2021: Climate Division Datasets (nClimDiv). NOAA, accessed 10 November 2021, https://www.drought.gov/data-maps-tools/climate-division-datasets-nclimdiv.

Fleming, S. W., 2007: An information theoretic perspective on mesoscale seasonal variations in ground-level ozone. *Atmos. Environ.*, **41**, 5746–5755, https://doi.org/10.1016/j.atmosenv.2007.02.027.

Freedman, A., 2012a: Causes of midwest drought: La Nina and global warming thought to contribute to dry weather. Huffpost, 21 July, https://www.huffpost.com/entry/causes-of-midwest-drought-2012_n_1690717.

——, 2012b: Drought in U.S. worsens, with no relief in sight. Climatecentral.org, 19 July, https://www.climatecentral.org/news/drought-worsens-with-no-relief-in-sight.

Gruber, A., T. Scanlon, R. van der Scalie, W. Wagner, and W. Dorigo, 2019: Evolution of the ESA CCI soil moisture climate data records and their underlying merging methodology. *Earth Syst. Sci. Data*, **11**, 717–739, https://doi.org/10.5194/essd-11-717-2019.

Heddinghaus, T. R., and P. Sabol, 1991: A review of the Palmer Drought Severity Index and where do we go from here?


Brought to you by NOAA Central Library | Unauthenticated | Downloaded 08/13/24 07:18 PM UTC

*Proc. 7th Conf. on Applied Climatology*, Salt Lake City, UT, Amer. Meteor. Soc., 242–246.

Heim, R. R., Jr., 2002: A review of twentieth-century drought indices used in the United States. *Bull. Amer. Meteor. Soc.*, **83**, 1149–1166, https://doi.org/10.1175/1520-0477-83.8.1149.

——, 2005: Computing the monthly Palmer Drought Index on a weekly basis: A case study comparing data estimation techniques. *Geophys. Res. Lett.*, **32**, L06401, https://doi.org/10.1029/2004GL022118.

Hobbins, M. T., A. Wood, D. J. McEvoy, J. L. Huntington, C. Morton, M. Anderson, and C. Hain, 2016: The Evaporative Demand Drought Index: Part I: Linking drought evolution to variations in evaporative demand. *J. Hydrometeor.*, **17**, 1745–1761, https://doi.org/10.1175/JHM-D-15-0121.1.

Hoell, A., and H. Wang, 2021: Flash drought prediction challenges and needs: Webinar on "state of the science" on flash drought. Drought.gov, https://www.youtube.com/watch?v=TH15W3zgxoM.

——, J. Perlwitz, and J. Eischeid, 2019: The causes, predictability, and historical context of the 2017 U.S. Northern Great Plains drought. Drought Assessment Rep., 27 pp., https://www.drought.gov/sites/default/files/2020-09/2017-NGP-drought-assessment.pdf.

Houborg, R., M. Rodell, B. Li, R. Reichle, and B. F. Zaitchik, 2012: Drought indicators based on model-assimilated Gravity Recovery and Climate Experiment (GRACE) terrestrial water storage observations. *Water Resour. Res.*, **48**, W07525, https://doi.org/10.1029/2011WR011291.

Huffman, G., and Coauthors, 2014: Integrated Multi-satellitE Retrievals for GPM (IMERG), version 6. NASA's Precipitation Processing Center, accessed 16 September 2021, https://gpm1.gesdisc.eosdis.nasa.gov/data/GPM_L3/GPM_3IMERGDF.06/.

Jain, V. K., and M. Sharma, 2003: Air quality monitoring network design using information theory. *J. Environ. Syst.*, **29**, 245–267, https://doi.org/10.2190/G518-4XQ4-BTNQ-KW9X.

Kraskov, A., H. Stögbauer, and P. Grassberger, 2004: Estimating mutual information. *Phys. Rev.*, **69E**, 066138, https://doi.org/10.1103/PhysRevE.69.066138.

Krasovskaia, I., 1995: Quantification of the stability of river flow regimes. *Hydrol. Sci. J.*, **40**, 587–598, https://doi.org/10.1080/02626669509491446.

——, 1997: Entropy-based grouping of river flow regimes. *J. Hydrol.*, **202**, 173–191, https://doi.org/10.1016/S0022-1694(97)00065-6.

Kreer, J., 1957: A question of terminology. *IRE Trans. Inf. Theory*, **3**, 208, https://doi.org/10.1109/TIT.1957.1057418.

Leopold, L. B., and W. B. Langbein, 1962: The concept of entropy in landscape evolution: Theoretical papers in the hydrologic and geomorphic sciences. USGS Professional Paper 500-A, 26 pp., https://pubs.usgs.gov/pp/0500a/report.pdf.

Lindsey, R., 2011: So far, Arctic Oscillation favoring mild winter for eastern U.S. Climate.gov., accessed 11 November 2021, https://www.climate.gov/news-features/featured-images/so-far-arctic-oscillation-favoring-mild-winter-eastern-us.

Lohmann, D., and Coauthors, 2004: Streamflow and water balance intercomparisons of four land surface models in the North American Land Data Assimilation System project. *J. Geophys. Res.*, **109**, D07S91, https://doi.org/10.1029/2003JD003517.

Luojus, K., J. Pulliainen, M. Takala, J. Lemmetyinen, and M. Moisander, 2020: GlobSnow v3.0 snow water equivalent (SWE). PANGAEA, accessed 26 September 2021, https://doi.org/10.1594/PANGAEA.911944.

Majda, A. J., and B. Gershgorin, 2010: Quantifying uncertainty in climate change science through empirical information theory. *Proc. Natl. Acad. Sci. USA*, **107**, 14 958–14 963, https://doi.org/10.1073/pnas.1007009107.

Maruyama, T., and T. Kawachi, 1998: Evaluation of rainfall characteristics using entropy. *J. Rainwater Catchment Syst.*, **4**, 7–10, https://doi.org/10.7132/jrcsa.KJ00003257785.

——, ——, and V. P. Singh, 2005: Entropy-based assessment and clustering of potential water resources availability. *J. Hydrol.*, **309**, 104–113, https://doi.org/10.1016/j.jhydrol.2004.11.020.

McEvoy, D. J., J. L. Huntington, M. T. Hobbins, A. Wood, C. Morton, M. Anderson, and C. Hain, 2016: The Evaporative Demand Drought Index: Part II: CONUS-wide assessment against common drought indicators. *J. Hydrometeor.*, **17**, 1763–1779, https://doi.org/10.1175/JHM-D-15-0122.1.

NASA/GSFC, 2021: NCA-LDAS specifications. NASA, accessed 29 May 2021, https://ldas.gsfc.nasa.gov/nca-ldas/specifications.

Nearing, G., S. Yatheendradas, W. Crow, X. Zhan, J. Liu, and F. Chen, 2018: The efficiency of data assimilation. *Water Resour. Res.*, **54**, 6374–6392, https://doi.org/10.1029/2017WR020991.

NOAA, 2023: North America Drought Indices and Indicators Assessment (NADIIA). North America Commission for Environmental Cooperation (CEC), accessed 1 February 2023, https://www.ncdc.noaa.gov/temp-and-precip/drought/nadiia/data.

NOAA/CPC, 2021: Experimental objective blends of drought indicators. NOAA, accessed 29 May 2021, https://www.cpc.ncep.noaa.gov/products/predictions/tools/edb/droughtblends.php.

NOAA/NCDC, 2021: nClimDiv dataset. NOAA, accessed 10 November 2021, https://www.ncdc.noaa.gov/monitoring-references/maps/us-climate-divisions.php#grdd.

NOAA/NCEI, 2021a: Gridded climate datasets: NOAA's nClimGrid-monthly. NOAA, accessed 10 November 2021, https://www.drought.gov/data-maps-tools/gridded-climate-datasets-noaas-nclimgrid-monthly.

——, 2021b: Climate division datasets (nClimDiv). NOAA, accessed 4 August 2020, https://www.ncei.noaa.gov/pub/data/cirs/climdiv/.

NOAA/NESDIS, 2021: STAR-Global vegetation health products: Downloading vegetation health products data. NOAA, accessed 8 October 2021, https://www.star.nesdis.noaa.gov/smcd/emb/vci/VH/vh_ftp.php.

NOAA/NIDIS, 2019a: Flash drought: Lessons learned from the 2017 drought across the U.S. Northern Plains and Canadian Prairies. Drought.gov Assessments/Rep., 76 pp., https://www.drought.gov/documents/flash-drought-lessons-learned-2017-drought-across-us-northern-plains-and-canadian.

——, 2019b: Flash drought: New reports examine the 2017 Northern Plains Drought. NOAA, accessed 26 October 2021, https://www.drought.gov/news/flash-drought-new-reports-examine-2017-northern-plains-drought.

——, 2021: What is flash drought? What can we do about it? NOAA, accessed 21 October 2021, https://www.drought.gov/news/what-flash-drought-what-can-we-do-about-it.

NOHRSC, 2004: Snow Data Assimilation System (SNODAS) Data Products at NSIDC, version 1. National Operational Hydrologic Remote Sensing Center, accessed 15 August 2021, https://doi.org/10.7265/N5TB14TC.

Null, J., 2023: El Niño and La Niña years and intensities. Accessed 11 March 2023, https://ggweather.com/enso/oni.htm.

Otkin, J. A., M. Svoboda, E. D. Hunt, T. W. Ford, M. C. Anderson, C. Hain, and J. B. Basara, 2018: Flash droughts: A review and assessment of the challenges imposed by rapid-onset droughts in the United States. *Bull. Amer. Meteor. Soc.*, **99**, 911–919, https://doi.org/10.1175/BAMS-D-17-0149.1.

Brought to you by NOAA Central Library | Unauthenticated | Downloaded 08/13/24 07:18 PM UTC

Pack, W., 2011: Drought rated as Texas' 3rd worst. MYSA, 8 June, https://www.mysanantonio.com/business/article/Drought-rated-as-Texas-3rd-worst-1416012.php.

Palmer, W. C., 1965: Meteorological drought. U.S. Weather Bureau Research Paper 45, 58 pp.

Preimesberger, W., T. Scanlon, C.-H. Su, A. Gruber, and W. Dorigo, 2021: Homogenization of structural breaks in the global ESA CCI soil moisture multisatellite climate data record. *IEEE Trans. Geosci. Remote Sens.*, **59**, 2845–2862, https://doi.org/10.1109/TGRS.2020.3012896.

Pulliainen, J., and Coauthors, 2020: Patterns and trends of Northern Hemisphere snow mass from 1980 to 2018. *Nature*, **581**, 294–298, https://doi.org/10.1038/s41586-020-2258-0.

Ross, B. C., 2014: Mutual information between discrete and continuous data sets. *PLOS ONE*, **9**, e87357, https://doi.org/10.1371/journal.pone.0087357.

Seager, R., and A. Tzanova, 2008: Drought in the southeastern United States: The recent drought in the context of a millennium of climate variability, physical changes, and future hydroclimate change. Lamont-Doherty Earth Observatory, http://ocp.ldeo.columbia.edu/res/div/ocp/drought/SE.shtml.

——, ——, and J. Nakamura, 2009: Drought in the southeastern United States: Causes, variability over the last millennium, and the potential for future hydroclimate change. *J. Climate*, **22**, 5021–5045, https://doi.org/10.1175/2009JCLI2683.1.

Shannon, C. E., 1948a: A mathematical theory of communication. *Bell Syst. Tech. J.*, **27**, 379–423, https://doi.org/10.1002/j.1538-7305.1948.tb01338.x.

——, 1948b: A mathematical theory of communication. *Bell Syst. Tech. J.*, **27**, 623–656, https://doi.org/10.1002/j.1538-7305.1948.tb00917.x.

Sonuga, J. O., 1972: Principle of maximum entropy in hydrologic frequency analysis. *J. Hydrol.*, **17**, 177–191, https://doi.org/10.1016/0022-1694(72)90003-0.

——, 1976: Entropy principle applied to the rainfall-runoff process. *J. Hydrol.*, **30**, 81–94, https://doi.org/10.1016/0022-1694(76)90090-1.

Svoboda, M., and Coauthors, 2002: The Drought Monitor. *Bull. Amer. Meteor. Soc.*, **83**, 1181–1190, https://doi.org/10.1175/1520-0477-83.8.1181.

Svoboda, M. D., B. A. Fuchs, C. C. Poulsen, and J. R. Nothwehr, 2015: The drought risk atlas: Enhancing decision support for drought risk management in the United States. *J. Hydrol.*, **526**, 274–286, https://doi.org/10.1016/j.jhydrol.2015.01.006.

Swain, D. L., and Coauthors, 2014: The extraordinary California drought of 2013/2014: Character, context, and the role of climate change, [in "Explaining Extremes of 2013 from a Climate Perspective"]. *Bull. Amer. Meteor. Soc.*, **95** (9), S3–S7, https://doi.org/10.1175/1520-0477-95.9.S1.1.

UNL, 2021a: USDM: This week's drought summary. UNL, accessed 2 November 2021, https://droughtmonitor.unl.edu/.

——, 2021b: NDMC Blends. UNL, accessed 29 May 2021, https://ndmcblends.unl.edu/.

van den Dool, H., J. Huang, and Y. Fan, 2003: Performance and analysis of the constructed analogue method applied to U.S. soil moisture over 1981–2001. *J. Geophys. Res.*, **108**, 8617, https://doi.org/10.1029/2002JD003114.

Vicente-Serrano, S. M., S. Beguería, and J. I. López-Moreno, 2010: A multiscalar drought index sensitive to global warming: The Standardized precipitation evapotranspiration index. *J. Climate*, **23**, 1696–1718, https://doi.org/10.1175/2009JCLI2909.1.

Vose, R. S., S. Applequist, I. Durre, M. J. Menne, C. N. Williams Jr., C. Fenimore, K. Gleason, and D. Arndt, 2014a: Improved historical temperature and precipitation time series for U.S. climate divisions. *J. Appl. Meteor. Climatol.*, **53**, 1232–1251, https://doi.org/10.1175/JAMC-D-13-0248.1.

——, and Coauthors, 2014b: NOAA Monthly U.S. Climate Divisional Database (NClimDiv). NOAA National Climatic Data Center, accessed 2 November 2021, https://www.ncei.noaa.gov/access/metadata/landing-page/bin/iso?id=gov.noaa.ncdc:C00005.

Wardlow, B., and Coauthors, 2017: The Quick Drought Response Index (QuickDRI)—A new tool for monitoring rapid changes in drought conditions. *23rd Conf. on Applied Climatology*, Asheville, NC, Amer. Meteor. Soc., 8B.2, https://ams.confex.com/ams/23Applied/webprogram/Paper318533.html.

WMO and GWP, 2016: Handbook of Drought Indicators and Indices (M. Svoboda and B. A. Fuchs). Integrated Drought Management Programme (IDMP), Integrated Drought Management Tools and Guidelines Series 2, WMO/TD-1173, 52 pp., https://www.droughtmanagement.info/literature/GWP_Handbook_of_Drought_Indicators_and_Indices_2016.pdf.

Woloszyn, M., and Coauthors, 2021: Flash Drought: Current Understanding and Future Priorities; Report of the 2020 NIDIS Flash Drought Virtual Workshop. NOAA National Integrated Drought Information System, 54 pp., https://www.drought.gov/sites/default/files/2021-07/NIDIS-Flash-Drought-Workshop-Report-2021.pdf.

Wrzesinski, D., 2016: Use of entropy in the assessment of uncertainty of river runoff regime in Poland. *Acta Geophys.*, **64**, 1825–1839, https://doi.org/10.1515/acgeo-2016-0073.

Xia, Y., M. B. Ek, D. Mocko, C. D. Peters-Lidard, J. Sheffield, J. Dong, and E. F. Wood, 2014: Uncertainties, correlations, and optimal blends of drought indices from the NLDAS multiple land surface model ensemble. *J. Hydrometeor.*, **15**, 1636–1650, https://doi.org/10.1175/JHM-D-13-058.1.

Yang, Y., and D. H. Burn, 1994: An entropy approach to data collection network design. *J. Hydrol.*, **157**, 307–324, https://doi.org/10.1016/0022-1694(94)90111-2.

Yatheendradas, S., and S. Kumar, 2022: A novel machine learning-based gap-filling of fine-resolution remotely sensed snow cover fraction data by combining downscaling and regression. *J. Hydrometeor.*, **23**, 637–658, https://doi.org/10.1175/JHM-D-20-0111.1.

Zaitchik, B. F., M. Rodell, and R. H. Reichle, 2008: Assimilation of GRACE terrestrial water storage data into a land surface model: Results for the Mississippi River basin. *J. Hydrometeor.*, **9**, 535–548, https://doi.org/10.1175/2007JHM951.1.

Zargar, A., R. Sadiq, B. Naser, and F. I. Khan, 2011: A review of drought indices. *Environ. Rev.*, **19**, 333–349, https://doi.org/10.1139/a11-013.

Brought to you by NOAA Central Library | Unauthenticated | Downloaded 08/13/24 07:18 PM UTC